AGU ADVANCING EARTH AND SPACE SCIENCES

Earth and Space Science

RESEARCH ARTICLE
10.1029/2023EA003485

Improving Equatorial Upper Ocean Vertical Mixing in the NOAA/GFDL OM4 Model

Brandon G. Reichl[1], Andrew T. Wittenberg[1], Stephen M. Griffies[1,2], and Alistair Adcroft[2]

[1]NOAA Geophysical Fluid Dynamics Laboratory, Princeton, NJ, USA, [2]Princeton University Program in Atmospheric and Oceanic Science, Princeton, NJ, USA

Key Points:

- Large eddy simulation results are used to evaluate the diurnal cycle of equatorial turbulent mixing in the OM4 ocean model
- Reducing vertical viscosity in an ocean model increases shear near the Equatorial Undercurrent (EUC) and can result in increased vertical mixing
- Vertical grid spacing of a few meters helps to resolve shear mixing events within and below the EUC in ocean models

Correspondence to:

B. G. Reichl,
brandon.reichl@noaa.gov

Citation:

Reichl, B. G., Wittenberg, A. T., Griffies, S. M., & Adcroft, A. (2024). Improving equatorial upper ocean vertical mixing in the NOAA/GFDL OM4 model. *Earth and Space Science*, *11*, e2023EA003485. https://doi.org/10.1029/2023EA003485

Received 21 DEC 2023
Accepted 26 JUL 2024

Abstract Deficiencies in upper ocean vertical mixing parameterizations contribute to tropical upper ocean biases in global coupled general circulation models, affecting their simulated ocean heat uptake and ENSO variability. To better understand these deficiencies, we develop a suite of ocean model experiments including both idealized single column models and realistic global simulations. The vertical mixing parameterizations are first evaluated using large eddy simulations as a baseline to assess uncertainties and evaluate their implied turbulent mixing. Global models are then developed following NOAA/GFDL's 0.25° nominal horizontal grid spacing OM4 (uncoupled) configuration of the MOM6 ocean model, with various modifications that target biases in the original model. We test several enhancements to the existing mixing schemes and evaluate them against observational constraints from Tropical Atmosphere Ocean moorings and Argo floats. In particular, we find that we can improve the diurnal variability of mixing in OM4 via modifications to its surface boundary layer mixing scheme, and can improve the net mixing in the upper thermocline by reducing the background vertical viscosity, allowing for more realistic, less diffuse currents. The improved OM4 model better represents the mixing, leading to improved diurnal deep-cycle variability, a more realistic time-mean tropical thermocline structure, and a better Pacific Equatorial Undercurrent.

Plain Language Summary Computational models of the oceanic and atmospheric circulation are critical tools for understanding and projecting changes in the Earth's climate. These models have errors that can arise from many sources, including model formulation or the choices in applying the model. One of the more well known sources of error is the representation of turbulent mixing. In this work we consider specially designed small-scale models that simulate turbulent mixing, and use their results to improve the representation of turbulence and its induced mixing in large-scale models. In particular, we investigate how the intensity of mixing varies throughout the day, considering the progression from deep mixing during cooler nighttime surface conditions to shallower mixing in the presence of strong solar heating during the day. We find some modifications to the mixing scheme in the ocean climate model that can improve the model solutions when compared to the real ocean.

1. Introduction

Coupled atmosphere-ocean general circulation models (CGCMs) are crucial tools for understanding and projecting the Earth's climate system and its response to changing climate forcings (IPCC, 2021). However, these models remain imperfect due to several factors, including their often coarse lateral and vertical resolution (to support timely production of seasonal forecasts and centennial projections) and incomplete parameterizations of unresolved physical processes (e.g., Fox-Kemper et al., 2019; Hawkins & Sutton, 2009; Hewitt et al., 2020; Palmer et al., 2005). Improving confidence in these models requires efforts on many fronts, and in this work we focus on the representation of upper ocean vertical mixing in the ocean general circulation model (OGCM) component of these CGCMs.

Vertical mixing in the upper ocean is particularly important for CGCMs, due to its role in mediating the exchange of mechanical energy, thermal energy, and other tracers (e.g., chemical compounds) between the atmosphere and ocean interior (see reviews by D'Asaro, 2014; Fox-Kemper et al., 2022; Large et al., 1994; Small et al., 2008). Vertical mixing also strongly influences rapid (e.g., diurnal to subseasonal) air-sea coupled processes (Price et al., 1986), as properties are most efficiently exchanged between the atmosphere and ocean turbulent boundary layers. At these time scales, the depth of the ocean surface boundary layer sets both the effective heat and

chemical capacity of the ocean (S. P. Anderson et al., 1996; Tozuka et al., 2018), and the inertial resistance of near-surface currents to acceleration by surface wind stresses (e.g., Hughes et al., 2020; Masich et al., 2021).

Ocean mixing processes in the tropical oceans play a key role in climate, since the large scale atmosphere-ocean coupled interactions that occur in this region affect the global heat balance and patterns of temperature and precipitation. A quintessential example of a coupled interaction is the El Niño/Southern Oscillation (ENSO) phenomenon (McPhaden et al., 2020), which is characterized by basin-scale changes in tropical Pacific sea surface temperature (SST), trade winds, currents, and patterns of upper ocean heat content. ENSO is one of the most important modulators of global climate patterns, through its various teleconnections (e.g., L'Heureux et al., 2015; X. Li et al., 2021; Ropelewski & Halpert, 1987; Sprintall et al., 2020; Taschetto et al., 2020; Trenberth et al., 1998). Simulating a realistic ENSO in a CGCM requires skill in simulating many relevant ocean and atmosphere processes, as well as the processes that govern the air-sea interface exchange (Guilyardi et al., 2020). It is therefore hypothesized that addressing deficiencies in upper ocean mixing of CGCMs can improve not only the simulated local ocean and atmosphere state, but also the simulated global climate, climate variability, and climate response of the model (Meehl et al., 2001; Richards et al., 2009).

One of the common upper ocean CGCM biases in the tropics is an overly strong and westward-shifted equatorial Pacific cold tongue (G. Li & Xie, 2014; Guilyardi et al., 2020), which interacts with other biases in the CGCM. The CGCM's simulated ocean SST near the equator is tightly connected to the strength, position, and watermass properties of its thermocline (G. Li & Xie, 2012), which results from a balance of atmospheric forcing, ocean vertical mixing physics, and resolved and parameterized advection. Atmospheric forcing directly affects the SST through its impact on surface heat and freshwater fluxes and radiation (e.g., via clouds, evaporation, and the diurnal cycle of shortwave radiation). The simulated winds also modulate the depth of the thermocline, due to Ekman pumping and Sverdrup transport induced by the wind stress (Chiodi & Harrison, 2017; Kessler, 2006; Voldoire et al., 2019), through transient adjustments via oceanic internal Rossby and Kelvin waves, and by helping to establish the large-scale lateral gradients of surface height and subsurface pressure. Ocean upwelling and vertical mixing processes also help to determine the patterns of SST and sea surface salinity (Farneti et al., 2022) by setting the vertical gradients of temperature, salinity, and density above the thermocline.

Numerous experiments have sought to characterize upper ocean turbulence near the equator, starting with observational efforts documented by Gregg et al. (1985) and Moum and Caldwell (1985), which were then followed by numerical LES studies (Pham et al., 2013; Wang et al., 1996, 1998; Whitt et al., 2022). Upper ocean vertical mixing near the equator modulates SST on timescales ranging from diurnal to seasonal and supports subsurface downward heat fluxes that may exceed 200 W/m^2 at ∼100 m depth close to the equator (Moum et al., 2013). The turbulence that drives this mixing is primarily energized by horizontal and vertical shear instability mechanisms (Moum et al., 2011; Peters et al., 1994; Smyth & Moum, 2013; C. Sun et al., 1998), with those currents including both time-mean and transient contributions from the local wind driven flow, tropical instability waves (TIWs), equatorial Kelvin waves, and basin-scale subsurface undercurrents such as the Equatorial Undercurrent (Cherian et al., 2021; Holmes & Thomas, 2015). The presence of a strong diurnal cycle of surface heating in the tropics strongly modulates the water column stability, driving a diurnal response in turbulence and mixing referred to as deep-cycle turbulence (Smyth & Moum, 2013).

As a primarily shear-driven turbulence, the potential for instability due to the mean flow is often characterized by weighing the stabilizing stratification (characterized by the buoyancy frequency $N^2 = -g\rho^{-1}\partial_z\rho$) against the kinetic energy available for mixing (characterized by the squared shear frequency $S^2 = (\partial_z u)^2 + (\partial_z v)^2$). The ratio of these is the gradient Richardson number:

$$\mathrm{Ri} = \frac{N^2}{S^2} = \frac{-g\partial_z\rho}{\rho\left((\partial_z u)^2 + (\partial_z v)^2\right)} \tag{1}$$

where g is the acceleration of gravity, ρ is the locally referenced potential density that depends on temperature, salinity, and local pressure, u and v are the zonal and meridional components of the current, and z is the upward geopotential coordinate. Ri = 0.25 is often taken as the critical value below which turbulent flows develop, based on stability analyses (Miles, 1961) and experimental data (e.g., Rohr et al., 1988). Observational campaigns have documented a diurnal variation of Ri that indicates the presence of marginally stable water (e.g., Ri slightly

greater than 0.25) from the near surface down to the thermocline during the day, that is rapidly destabilized (Ri < 0.25) at night (e.g., Smyth & Moum, 2013). At night, this downward destabilization is fed by a downward flux of shear that propagates turbulence, momentum, and heat from the warm surface layer to cooler waters at depth, frequently approaching 100 m at 140°W (Smyth et al., 2013). Similar patterns have been observed in long term turbulence measurements in both the Pacific and Atlantic basins (Moum et al., 2022; Wenegrat & McPhaden, 2015), and likely also occur in the Indian Ocean (Pujiana et al., 2018).

While the characteristics of this turbulence are now fairly well known from observations and process models, the connection to the mean flow and turbulent fluxes in CGCMs requires accurate turbulence closure parameterizations to properly capture the spatiotemporal patterns and state-dependence (see Pei et al., 2020). Approaches to parameterize upper ocean turbulence vary among different OGCMs, where it is relatively common to employ bulk models for the boundary layer that are coupled to interior shear mixing schemes below (Large et al., 1994; Reichl & Hallberg, 2018). Comparing the various bulk approaches with one or two-equation turbulent kinetic energy (TKE) based schemes confirms that there is significant uncertainty remaining in representing vertical mixing processes in ocean models (Q. Li et al., 2019). A key part of resolving this uncertainty is careful evaluation of various mixing schemes against high-fidelity LES, which is one goal of this study. A further complication is the expectation that vertical resolution capable of resolving detailed structure of mean vertical shears may be required to achieve optimal performance from present vertical mixing schemes. For example, Jia et al. (2021) used grid spacing of 3 m in the upper 400 m, with the impact of vertical resolution on mixing also examined in this work.

Here we study how parameterized upper ocean mixing processes in the ocean component of a recent-generation CGCM (e.g., part of the Coupled Model Intercomparison Project 6, or CMIP6 era, see Eyring et al. (2016)) represent tropical mixing patterns and stratification, and investigate the impact of improved mixing on biases in the ocean mean state and variability. Although our ultimate goal is to improve the representation of upper ocean stratification and circulation via ocean mixing in CGCMs, our first step is to investigate the sensitivity of the ocean component to changes in mixing under atmospheric forcing arising from a prescribed atmospheric state. In Section 2 we describe the ocean configuration, namely the NOAA Geophysical Fluid Dynamics Laboratories Ocean Model 4 (OM4, Adcroft et al., 2019), and discuss its key upper ocean physics parameterizations used within OM4 that are investigated in this work. In Section 3 we utilize a recent LES study of turbulence near the equator at 140°W (Whitt et al., 2022), to evaluate the turbulent fluxes predicted by OM4 in a one-dimensional column model configuration. In Section 4 we follow the LES exercise by analyzing several additional changes required in OM4 to improve the simulated tropical currents and stratification. We conclude with a summary and future outlook for improved mixing schemes in CGCMs (Appendix A).

2. OM4 and Baseline Evaluation

Forced OGCM simulations, where the atmospheric fields are not interactive (e.g., following the 2nd Ocean Model Intercomparison Protocol OMIP2, Griffies et al., 2016; Tsujino et al., 2020), provide an approach to assess ocean model biases in a simpler context than CGCMs. The reason we employ this approach is partially to simplify the analysis by avoiding the complex coupled feedbacks and chaotic variability that occur in CGCMs (which require long runs or large ensembles to sample adequately). We also assume that since the winds in the reanalysis products are constrained by observations, they should be closer to nature than those from CGCMs. This assumption may be somewhat flawed, since the reanalyses used to drive OMIP style simulations contain their own biases (Taboada et al., 2019), which contribute to specific circulation biases in the tropics (e.g., Z. Sun et al., 2019). Atmosphere-ocean coupled feedbacks also modulate the characteristics of TIWs (Seo et al., 2007), but are absent in OGCMs, which in turn may affect model representation of TIW associated vertical mixing (see Cherian et al., 2021; Jochum & Murtugudde, 2006). Further complicating the use of OMIP runs to assess ocean sensitivities is that the ocean biases may not have the same magnitude or even sign as in the CGCM (see Adcroft et al., 2019, also demonstrated later in this section). Despite these qualifiers, current generation forcing data sets, such as the JRA55-do product developed during OMIP2 (Tsujino et al., 2018), represent a practical first step to produce realistic ocean simulations for comparisons over the recent historical epoch.

The base OMIP2 simulations studied here use NOAA Geophysical Fluid Dynamics Laboratory's (GFDL) OM4 ocean and sea-ice model (Adcroft et al., 2019), which is a coupled configuration of the Modular Ocean Model 6 (MOM6) and Sea Ice Simulator 2 (SIS2) code bases. OM4 is used as the ocean and sea-ice components of GFDL's CM4 CGCM (Held et al., 2019), and closely resembles the ocean and sea-ice components of GFDL's ESM4.1

(Dunne et al., 2020) and Seamless System for Prediction and Earth System Research (SPEAR, Delworth et al., 2020) CGCMs. Hence, the improvements to ocean mixing physics investigated here can readily inform the future development of GFDL's coupled climate models and forecast systems. In the following subsection we describe only the most relevant OM4 settings, focusing on those examined in this study. For a complete description of OM4, see Adcroft et al. (2019).

2.1. Model Description

2.1.1. Initialization and Forcing Protocol

Unless otherwise noted, we follow the same approach as OM4 for model configuration choices, including a nominally 0.25° tripolar horizontal grid, and a hybrid z^* (stretched geopotential) and σ_2 (potential density referenced to 2,000 dbar) vertical coordinate (e.g., OM4p25, see Adcroft et al., 2019). The initial potential temperature and salinity are interpolated to the model grid from January of the 2005 World Ocean Atlas historical climatology (Locarnini et al., 2006; Mishonov et al., 2006). For forcing, we apply the most recent JRA55-do reanalysis product (version 1.5), which is an update from the OMIP2 forcing of Tsujino et al. (2018) including some bugfixes and additional years (we present results through the end of 2018). The JRA55-do forcing provides lower atmosphere values needed for computing bulk air-sea fluxes (see Large & Yeager, 2009), including the near surface temperature, humidity, pressure, and winds at 3 hr intervals with a horizontal spacing of approximately 0.5°. The JRA55-do forcing also provides longwave and shortwave heat fluxes as well as freshwater fluxes at similar intervals. We employ the same sea surface salinity restoring to climatology as Adcroft et al. (2019), with the restoring piston velocity set to 0.1667 m day^{-1} (e.g., 300 days e-folding time for a 50 m thick slab). Tropical ocean stratification is also sensitive to parameterized shortwave penetration (e.g., Gnanadesikan & Anderson, 2009). OM4 estimates shortwave penetration profiles using the optical model of Manizza et al. (2005), together with a monthly chlorophyll climatology (see Adcroft et al. (2019) for detail).

2.1.2. OM4 Mixing Parameterizations

The ocean surface boundary layer is a particularly important region of vertical mixing, which is often represented in ocean models using combinations of parameterizations for different physical processes. There are numerous ocean physics parameterizations within MOM6 that are used by OM4, which play significant roles in its simulated ocean currents and hydrography in the top several hundred meters of the tropical oceans. Vertical fluxes in OM4's ocean surface boundary layer are provided via eddy mixing coefficients from the ePBL (energetic Planetary Boundary Layer) mixing parameterization (Reichl & Hallberg, 2018). These ePBL mixing coefficients are supplemented by an interior stratified shear mixing scheme, which follows the TKE-diffusivity mixing scheme described in Jackson et al. (2008) (hereafter JHL). The vertical mixing predicted in OM4 by ePBL and JHL is tested in detail in this study using LES reference simulations in Section 3, resulting in a proposed mixing formulation that reduces biases relative to the OM4 configuration. The vertically homogenizing turbulent fluxes primarily originate from ePBL and JHL in the upper ocean, and are opposed by submesoscale mixed layer eddy (MLE) restratification, which is parameterized as described by Fox-Kemper et al. (2011).

Interior mixing in OM4 is also parameterized using several different schemes that represent effects of different physical processes. The interior background vertical diffusivity in OM4 is determined by the latitude, as motivated by internal wave properties and described in Harrison and Hallberg (2008), which yields a background vertical diffusivity of temperature and salinity increasing from 2×10^{-6} m^2 s^{-1} at the equator to 1.15×10^{-5} m^2 s^{-1} at ±60° latitude. The background vertical viscosity is initially set equal to the vertical tracer diffusivity (i.e., the Prandtl number is assumed to be 1.0). In the original OM4, this viscosity is then supplemented with an additional constant background vertical viscosity of 10^{-4} m^2 s^{-1} everywhere. In Section 4 we examine the effects of this additional constant background vertical viscosity, which results primarily from historical convention and is not linked to a specific physical process. Finally, horizontal eddy mixing of momentum is achieved with a biharmonic Smagorinsky lateral viscosity (Griffies & Hallberg, 2000); there is no additional parameterized lateral mixing of tracers.

2.1.3. OM4 z_* and Virtual Moorings

To aid comparison of the OM4 model output with mooring data in Section 4, we conduct an additional set of OM4 simulations with a few changes. We shift from the hybrid ($z_* - \sigma_2$) coordinate of the OM4 model to a purely z_*

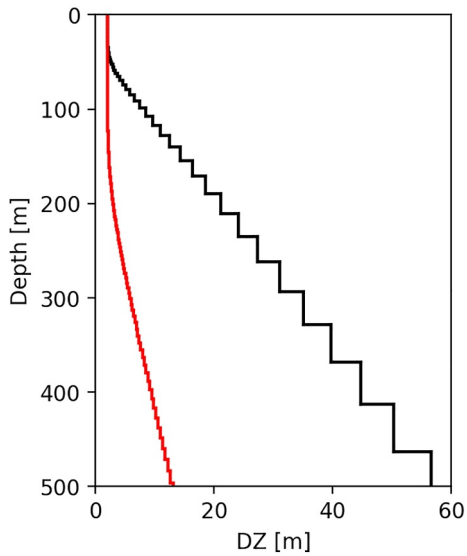

Figure 1. OM4's vertical grid spacing as a function of depth, for the upper-ocean z_* component of the vertical coordinate (note the resulting OM4 hybrid coordinate vertical grid spacing also depends on the σ_2 component). The black line represents the original z_* coordinate with 75 levels, and the red uses the same vertical grid spacing near the surface but with 225 total levels.

coordinate, which is done to maintain a specified vertical grid spacing (2 m telescoping spacing, see black curve in Figure 1) in the upper ocean for computing vertical gradients.

Changing to a z_* coordinate does impact the OM4 simulation in the tropics, since the hybrid coordinate produces coarse levels that frequently exceed 50 m spacing within the weakly-stratified upper 200 m in the west Pacific. These coarse layers affect the resolution of the vertical stratification and shears that are used in the mixing parameterizations. The z_* based version of OM4 also has more spurious mixing in regions of sloping isopycnals than the hybrid coordinate model (see Adcroft et al., 2019), which is a trade-off deemed necessary to improve the vertical resolution in this study from the hybrid coordinate in the Western Pacific. The differences between the z_* and hybrid coordinate OM4 model can be significant below 500 m and on long timescales (Adcroft et al., 2019), so we primarily focus on the upper few hundred meters and shorter simulations in this analysis. We comment more on the concerns related to the vertical coordinate in Section 5, and direct the reader to Adcroft et al. (2019) for further discussion of numerical mixing and model differences in the z_* model.

The OM4z_* models are rerun from the World Ocean Atlas initial condition starting in 1999, and run through 2008; only the 2001–2008 epoch is analyzed, to omit the initial spinup effects. We extended one OM4z_* simulation to 2022, and confirmed that the analysis through 2008 is sufficient to yield robust statistics. We implemented virtual mooring outputs into the OM4z_* model, to output 2-hr averaged model profiles every 2 hr. In Section 5, we introduce a refined vertical grid (Figure 1), with triple the number of vertical levels (from 75 to 225) relative to the standard OM4 model. The refined vertical grid spacing is less than 20 m throughout the top 500 m of the ocean, spanning the vertical range of the equatorial thermocline and EUC.

2.2. Climatological OM4 Equatorial Stratification Bias

We next describe the baseline biases in OM4, simulated using the OMIP2 protocol with the JRA55-do atmospheric forcing. We first examine the equatorial longitude-depth section of temperature and salinity, averaged from 1°S to 1°N (Figure 2). The observational product chosen for comparison is based on the updated (through 2022) Argo ocean state estimates (Roemmich & Gilson, 2009), though a similar comparison could be found with model based reanalysis products for the climatology (e.g., Chang et al., 2013).

OM4's equatorial SST is generally warmer than observed in all three basins (Figure 2e). Each basin also shows subsurface temperature biases linked to vertical displacements of the equatorial thermocline, with OM4 producing a shallower thermocline in the east Pacific and east Indian Oceans, a more intense thermocline in the west Pacific, and a deeper thermocline in the east Atlantic. A notable interbasin difference is that the bulk of the interior (e.g., 100–500 m) is too warm in the equatorial Indian ocean (corresponding to a thicker thermostad below the thermocline), but too cold in the Pacific and Atlantic (corresponding to a thinner thermostad below the thermocline). OM4 is saltier than Argo at the surface, except in the rainy zones near the Maritime Continent (Figure 2f). OM4 also shows a much saltier EUC in the Pacific, compared to Argo. Below 200 m, OM4 produces fresh biases in the Atlantic and Pacific, and salty biases in the Indian Ocean.

The corresponding OM4 biases in thermal and haline vertical stratification ($\partial_z\theta$ and $\partial_z S$) also show dependence on depth and basin (Figure 3). The Indian ocean basin again looks distinct from the Pacific and Atlantic Ocean basins. The OM4-simulated equatorial Indian ocean shows excessive thermal stratification between 50 and 100 m, and insufficient thermal stratification between 100 and 150 m, roughly corresponding to a shoaling of the thermocline (Figure 3e). In the equatorial Pacific and Atlantic, OM4 simulates a thermocline that is too shallow near the eastern boundaries, and too diffuse over the remainder of these basins. The salinity stratification is also strong in OM4, with excessive negative $\partial_z S$ near the surface in the western Atlantic and Pacific basins, above regions of excessive positive $\partial_z S$ (Figure 3f). These stratification biases suggest that there may be too little vertical

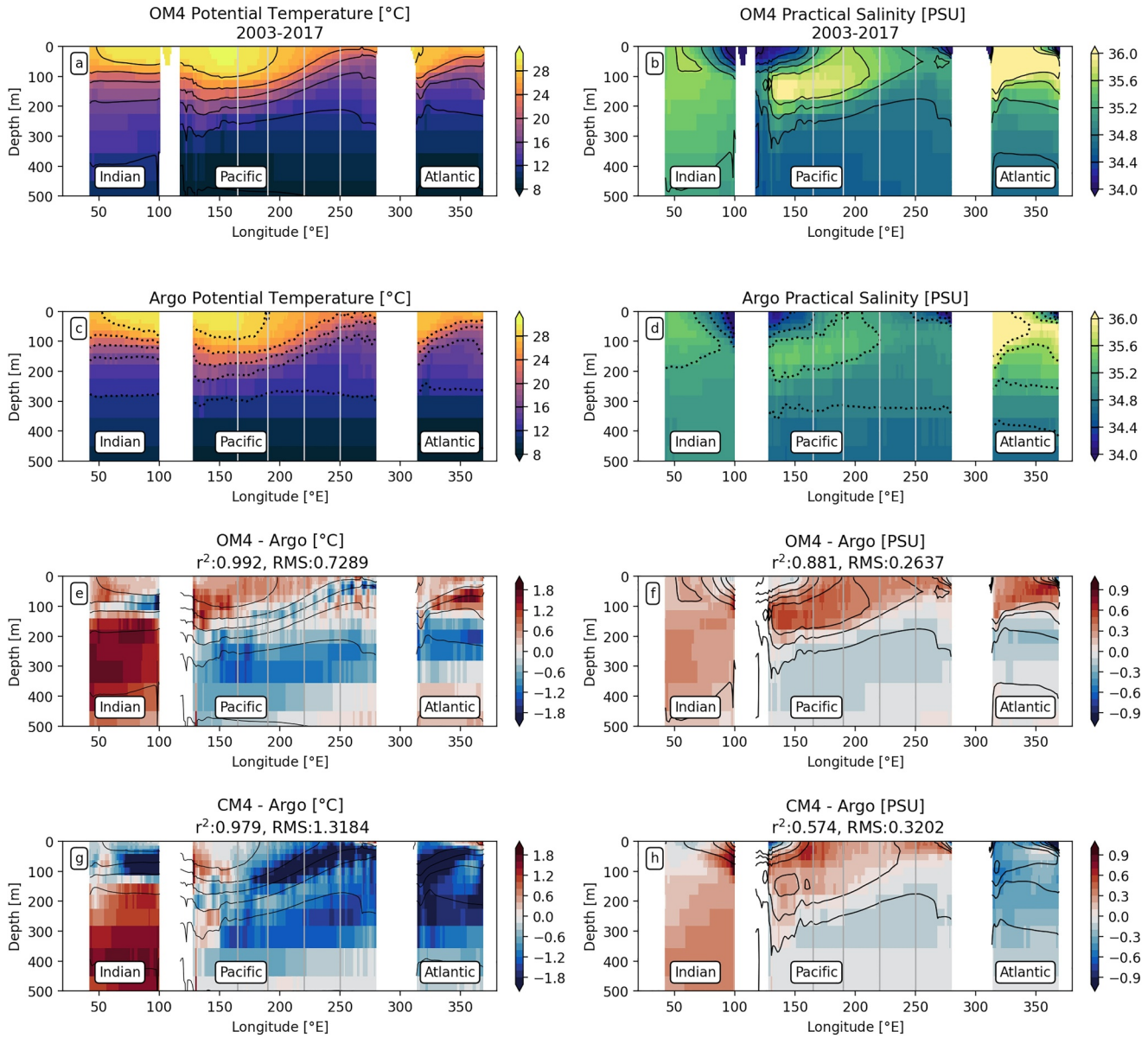

Figure 2. OM4 climatological potential temperature (panel a) and practical salinity (panel b); similar from Argo climatology (panels (c and d), 2004–2020, Roemmich and Gilson (2009)); the respective differences (OM4 minus Argo, panels (e and f); and the CM4 minus Argo differences (panels (g and h)), all averaged from 1°S to 1°N. The panel titles for the bias maps include the r^2 (Pearson correlation coefficient squared) and RMSE (square root of the mean square error) difference metrics. In (a–d), the shading is incremented every 1°C or 0.1 PSU; every fourth increment is also contoured in black (4°C or 0.4 PSU, solid for model, dashed for observation), as indicated on the colorbars. To aid comparison, the model contours are repeated in (e and f). The vertical lines indicate mooring locations at 165°E, 170°W, 140°W, and 110°W, which are discussed in Section 4.

mixing by ePBL/JHL, and/or too much restratification by MLE, in OM4's upper ocean. We show in Section 4 that these biases are improved with additional vertical mixing associated with more vertical shears in JHL.

2.3. Comparing the OM4 and CM4 Tropical Stratification Biases

For reference to the CM4 CGCM counterpart to OM4, we briefly contrast the OM4 equatorial transect biases to the CM4 biases (see also Figure 30g and 30h of Held et al. (2019)). The CM4 temperature and salinity biases from Argo are also shown in Figure 2 and similar maps for stratification are shown in Figure 3. As explained in Adcroft et al. (2019), OM4 and CM4 do not have the same sign SST bias at the equator (which remains true here with JRA55-do v1.5 forcing), and this difference can be seen to apply throughout the upper 500 m of these simulations.

10.1029/2023EA003485

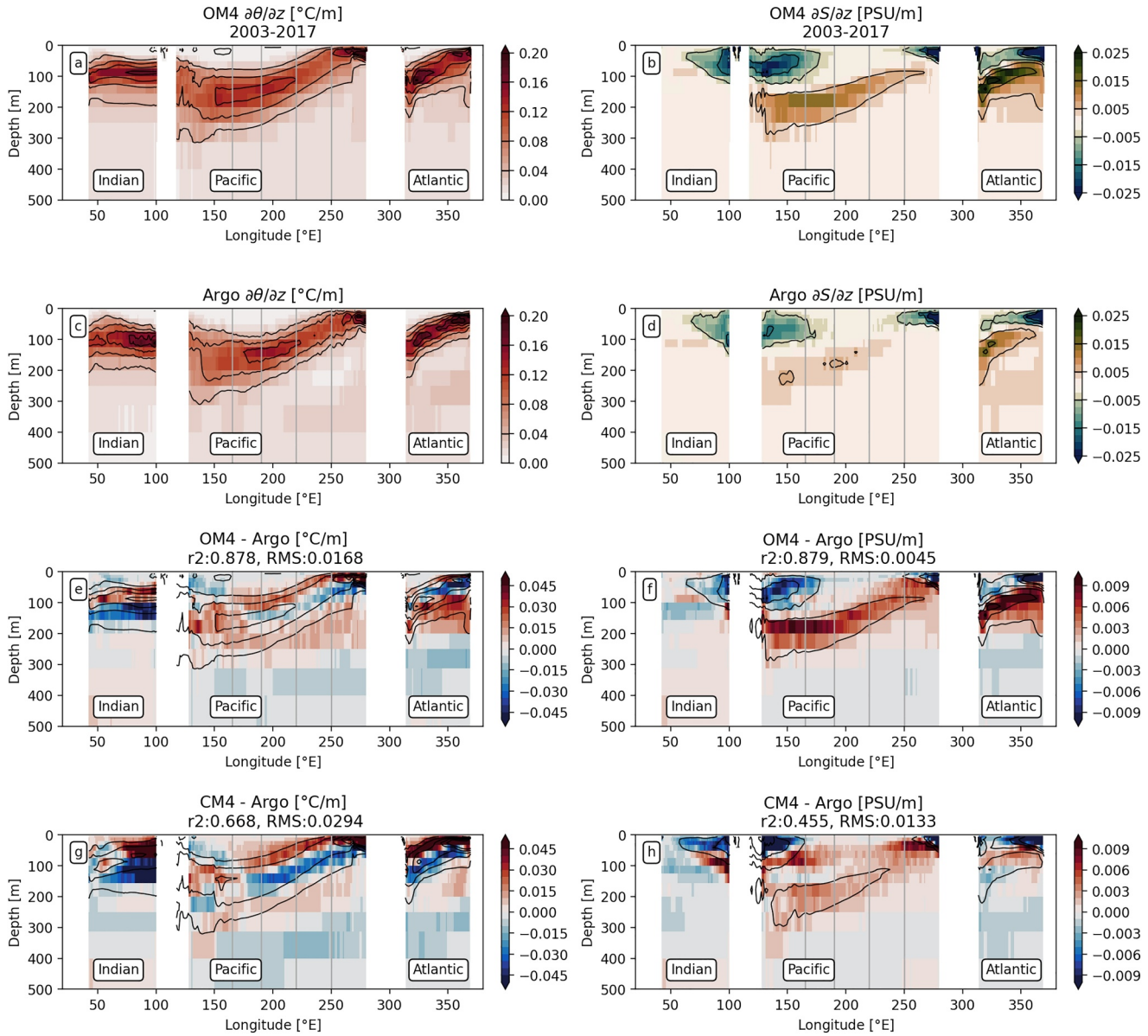

Figure 3. As in Figure 2, but for the vertical derivatives of temperature and salinity.

CM4 is significantly colder in the upper parts of all basins, though the warm Indian basin bias at depth is common to OM4 and CM4. Since the ocean component of these models is the same, these differences must be linked to differences in the ocean-atmosphere fluxes — arising from either the atmospheric model component, or its response to the OGCM-generated SSTs, or from subsequent coupled ocean-atmosphere interactions that can modify biases seeded by either component.

The stratification biases are significantly worse in CM4 than OM4, but generally show similar patterns, suggesting that these coupled biases may partly originate from OM4 rather than the atmospheric component. In particular, the excessive stratification in the shallow waters along the equator (in all three eastern equatorial basins), and the shoaling of the equatorial thermocline relative to observations, are similar between OM4 and CM4. Since stratification is directly impacted by vertical mixing, the common biases observed here between OM4 and CM4 suggest that the time-mean stratification could be a useful metric to evaluate the impact of ocean mixing parameterizations, which may yield relatively consistent impacts in both the OGCM and CGCM.

3. Evaluating Upper Ocean Parameterizations in Equatorial Regions in OM4: An LES Approach

In situ ocean observations of properties like temperature, salinity, and current speeds are an optimal basis for evaluating numerical ocean model simulations. However, directly testing ocean mixing schemes at the process level has traditionally been conducted using idealized, high resolution numerical models, especially LES. A recent process study by Whitt et al. (2022) presents a realistic pair of tropical LES in the region of interest for this study, which are thus chosen to assess the upper ocean mixing in the baseline OM4 model. In Whitt et al. (2022), these LES solutions were evaluated extensively in comparison to mooring estimated vertical turbulent heat fluxes.

This set of LES is formulated to resolve the one-dimensional (vertical) turbulent mixing processes that are parameterized in OGCMs like OM4. However, in the equatorial oceans the vertical mixing is significantly modulated by large-scale horizontal processes ($>10^6$ m) that are not captured at the horizontal scales of the LES domain ($\leq 10^4$ m). The effects of these large-scale processes are included by prescribing time-varying profiles of the time-tendencies of ocean currents, temperature, and salinity into the LES equations. These tendencies are extracted from the output of a separate three-dimensional regional model that spans the equatorial Pacific domain (see Whitt et al., 2022). To facilitate a comparison between OM4's vertical mixing and the LES, we therefore implement the capability in MOM6 to read the same external forcing time-tendency terms for temperature, salinity, and momentum, following Whitt et al. (2022). This method allows the one-dimensional (column) version of OM4 (OM4-1d) to represent the large-scale circulation impacts on turbulence in the same idealized way as the LES experiments, including just the one-way impact of the EUC shear on the local turbulent production, and omitting any feedbacks of the local turbulence onto the large-scale drivers of EUC shear. We conduct OM4-1d simulations with the same 0.5 m vertical grid spacing as the LES.

3.1. Comparison of OM4-1d and LES

We start by confirming that the OM4-1d and LES models produce a similar mean temperature and current structure (Figure 4). The figure shows the evolution of temperature and zonal current at 140°W during the 35 days simulation, which runs from 2 October 1985 to 6 November 1985. Compared to the LES, OM4-1d does a reasonable job simulating the temperature and current evolution at both the equatorial and 3°N sites.

To more directly examine the impact of the parameterized mixing in OM4-1d versus the LES, we next examine the time series of turbulent vertical temperature (heat) flux and the Richardson number, over a 7 day time slice (28 October through 5 November) from the full experiment (Figure 5). The main patterns are similar between the LES and OM4-1d, which is not surprising given the agreement in the mean temperature. Yet, there is a very clear difference in the diurnal variation and vertical structure of the vertical temperature fluxes. Of particular note is the more rapid downward penetration of the temperature flux each night, which yields more rounded structures in the vertical temperature fluxes in OM4-1d. In the LES the temperature flux penetration each night occurs more gradually, resulting in sharper, pointed features and induced tendencies than in OM4-1d. The Richardson number also has a more pronounced oscillation between large and small values in OM4-1d than in the LES, in the upper 10 m at the equator (third row) and the upper 35 m at 3°N (bottom row).

To better understand these differences we diurnally composite both the vertical temperature flux field and the gradient Richardson number (Figure 6). The composites show a repeated daily cycle of temperature flux and Richardson number, centered at the local noon (hour zero) peak of solar heating. The downward temperature flux in the LES (panels a and b) preserves the regular peaked structure, while the rounded nature of the OM4-1d (panels e and f) is seen in both the raw time series data and the diurnal composite. The OM4-1d temperature flux predicts excessive downward temperature fluxes in the upper 30 m at hour 0, which is when the LES shows a near complete shutdown of vertical mixing. This mixing is associated with a deep ePBL boundary layer in OM4-1d, indicated by the black line. The column Richardson number also reflects a bias in the OM4-1d result (panels g and h). Most notably, OM4-1d has an excessively rapid deep penetration of vertically unstable water (small/negative Ri) at night, and a rapid and excessive stabilization (large Ri) during the day. The LES Richardson number oscillates around $Ri = 0.25$ much more gradually, which is also consistently found in observations (e.g., Smyth & Moum, 2013). We conclude from these comparisons that a major bias emerges in the diurnal pattern of OM4 vertical mixing and column stability.

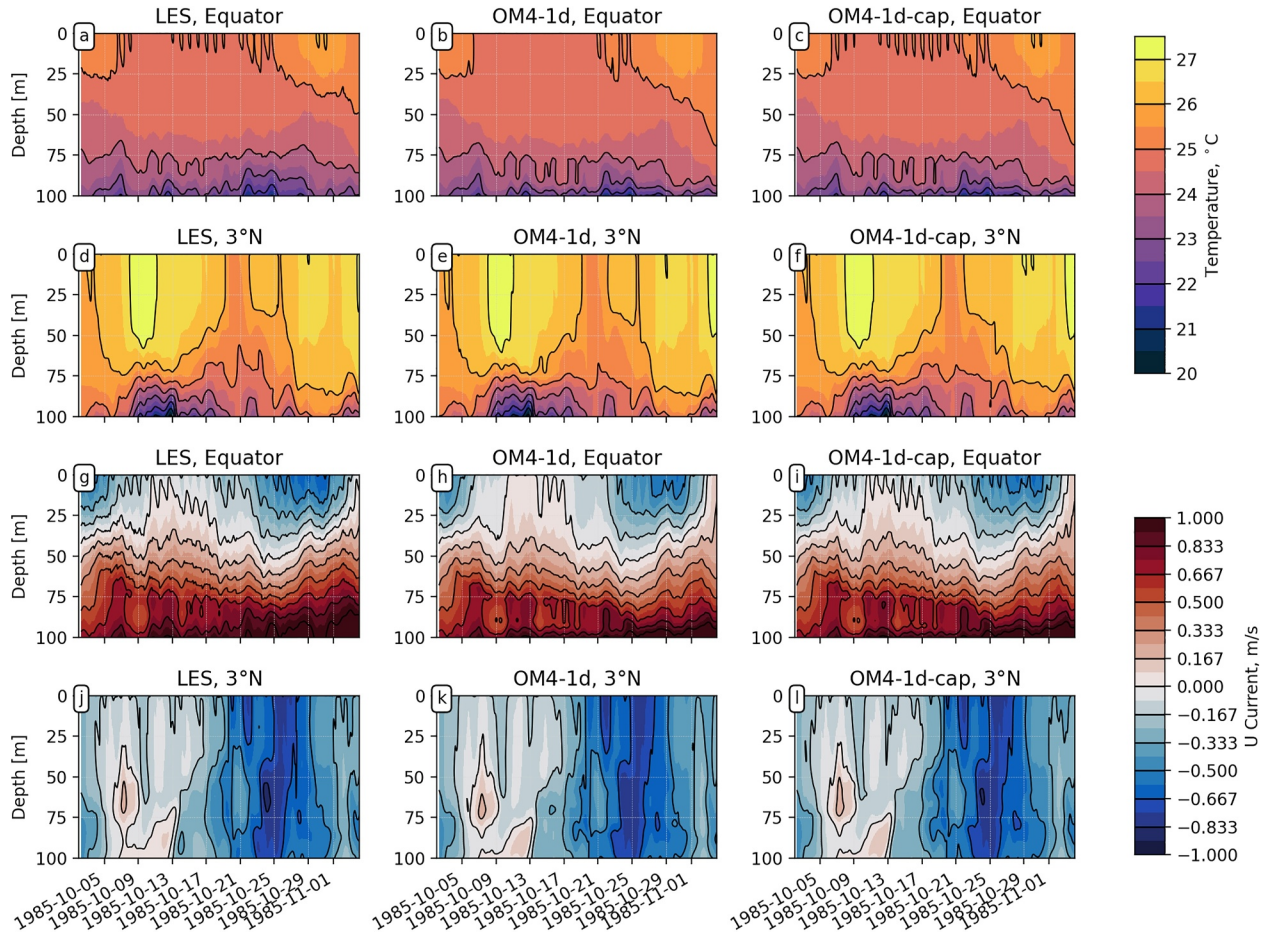

Figure 4. Large eddy simulation (LES) (left column), OM4-1d (middle column), and OM4-1d-cap (right column) simulations of upper-ocean temperature (upper two rows) and zonal velocity (lower two rows) at 140°W, for the equatorial (first and third row) and 3°N (second and fourth row) sites. LES provided from Whitt et al. (2022).

3.2. Improved OM4-1d for Simulating Deep Cycle Turbulence

3.2.1. Modification to ePBL, m_* Cap

The ePBL mixing energy is parameterized from $m_* u_*^3$, where m_* is the proportionality between the vertically integrated rate of conversion between TKE and potential energy (due to turbulent mixing in gravitationally stable stratification), and u_* is the wind friction velocity. The m_* parameterization used by OM4-1d significantly overestimates the daytime net vertical temperature flux in the upper 30 m, as demonstrated at hour 0 in Figure 6. We now explain the reason for this disagreement between the ePBL temperature flux and the LES, and offer a strategy to improve the diurnal cycle of the vertical mixing in OM4. The ePBL mixing scheme constrains the depth of the ocean surface boundary layer, based on the energetics associated with turbulent mixing of a stratified fluid (Reichl & Hallberg, 2018). In Reichl and Hallberg (2018), the parameterization for mixing energy is developed using numerical experiments that experience constant surface forcing (wind stress and surface bouyancy fluxes). The resulting parameterization therefore satisfies a condition where the boundary layer depth, buoyancy flux, and mechanical forcing terms all vary relatively slowly in time. The mean properties (e.g., shear and stratification) are not explicitly considered by ePBL, and instead the turbulent fields are parameterized only using information about the surface forcing and the boundary layer depth.

The overestimation of the temperature flux in the daytime by ePBL happens when there is a rapid change in the forcing conditions, mean shear and stratification, and the boundary layer depth over the diurnal cycle. This rapid change means that these quantities are never in equilibrium, and so the turbulence can no longer be reliably parameterized solely from the surface forcing. For example, as the sun rises, the boundary layer can remain deep

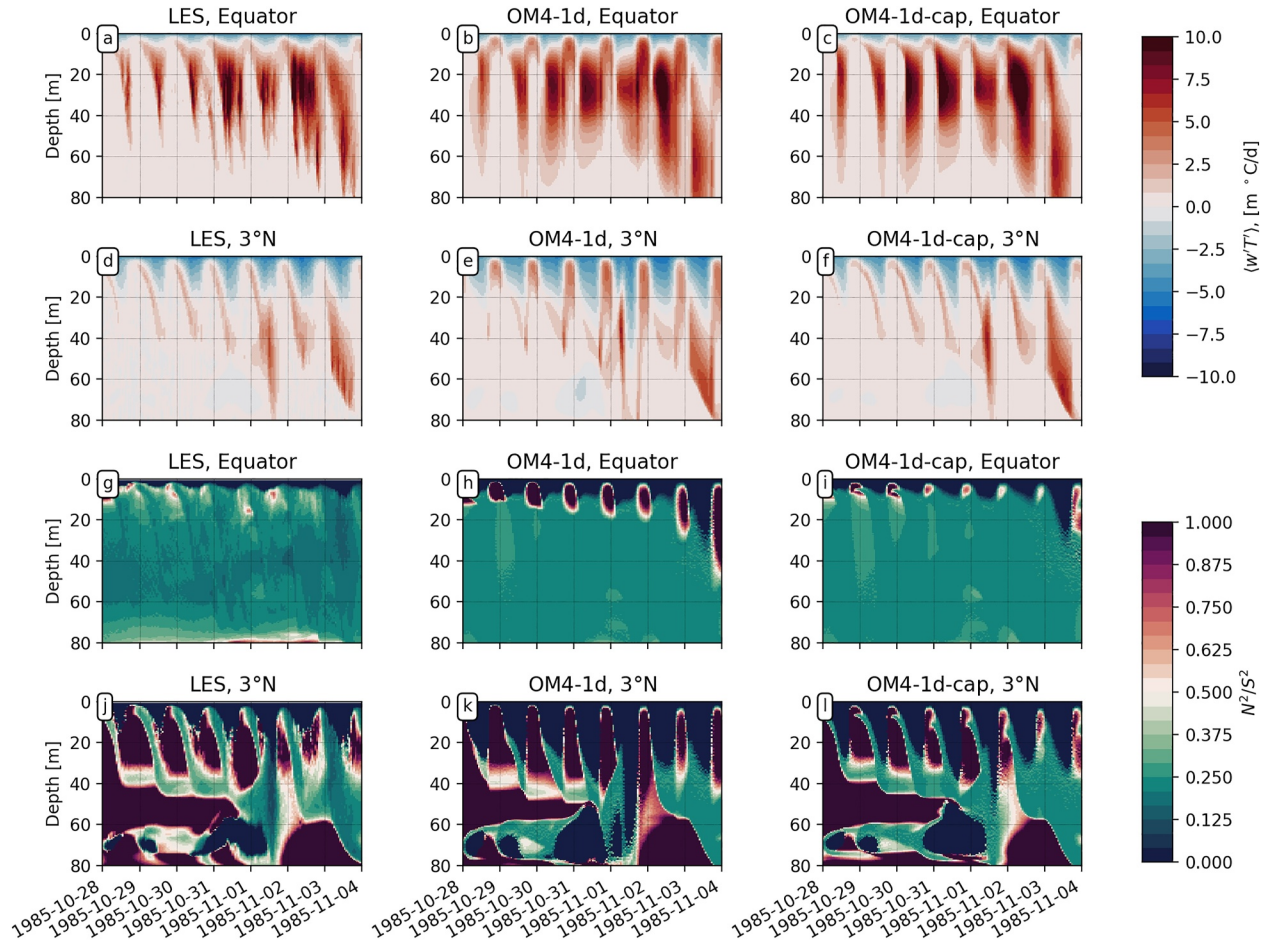

Figure 5. One-week subset of large eddy simulation (LES) (left column), OM4-1d (middle column), and OM4-1d-cap (right column) simulations of vertical turbulent temperature flux (positive downward, upper two rows) and gradient Richardson number ($\mathrm{Ri} = N^2/S^2$, lower two rows) at 140°W, for the equatorial (first and third row) and 3°N (second and fourth row) sites. LES provided from Whitt et al. (2022). The Ri colormap saturates at zero and one, but can be negative or much greater than one.

for a few hours, due to pre-existing ("fossil") turbulence from the night before. In this situation, the Reichl and Hallberg (2018) mixing energy parameterization (which scales the energy according to the boundary layer depth) would overestimate the mixing energy, since the boundary layer can remain deep despite the strong solar heating at the surface. Hence, the m_* predicted by ePBL is only accurate after the stable buoyancy gradient has been established, and the boundary layer depth has fully adjusted to the surface forcing conditions.

The assumptions that underpin ePBL's predictions of boundary layer depths can break down in near-equatorial regions with marginal stability and rapidly changing conditions, making it difficult to determine a suitable prescription for m_*. However, separate column model tests reveal that by setting m_* to zero at the equator in ePBL, and thus only using the JHL shear driven mixing scheme in this region, the OM4-1d model can predict downward heat fluxes and temperatures that are much more similar to the LES. Indeed the JHL scheme is well suited for predicting diffusivities for shear-driven mixing processes, which dominate the turbulence within this region. Additional tests (not shown) of the ePBL m_* prescription in the column model reveal a practical fix for the overmixing: namely, capping the ePBL m_* at a value close to 1, but much less than 10. Additional sensitivity studies suggest that 1.25 is a reasonable choice for this cap, and indeed the value of m_* outside ±5° is nearly always less than 1.25. For the present study, then, prescribing $m_* \leq 1.25$ appears to be a practical and reasonable approach to improve the equatorial simulation, without degrading the performance of ePBL outside of this region. Future work will focus on more physically-based estimates of m_* and its interaction with JHL in the tropics and elsewhere.

Figure 5 (3rd column) and Figure 6 (3rd row) demonstrate that this m_* cap significantly improves the diurnal phasing of the ePBL boundary layer depth and OM4 temperature flux (experiment OM4-1d-cap). We see that

10.1029/2023EA003485

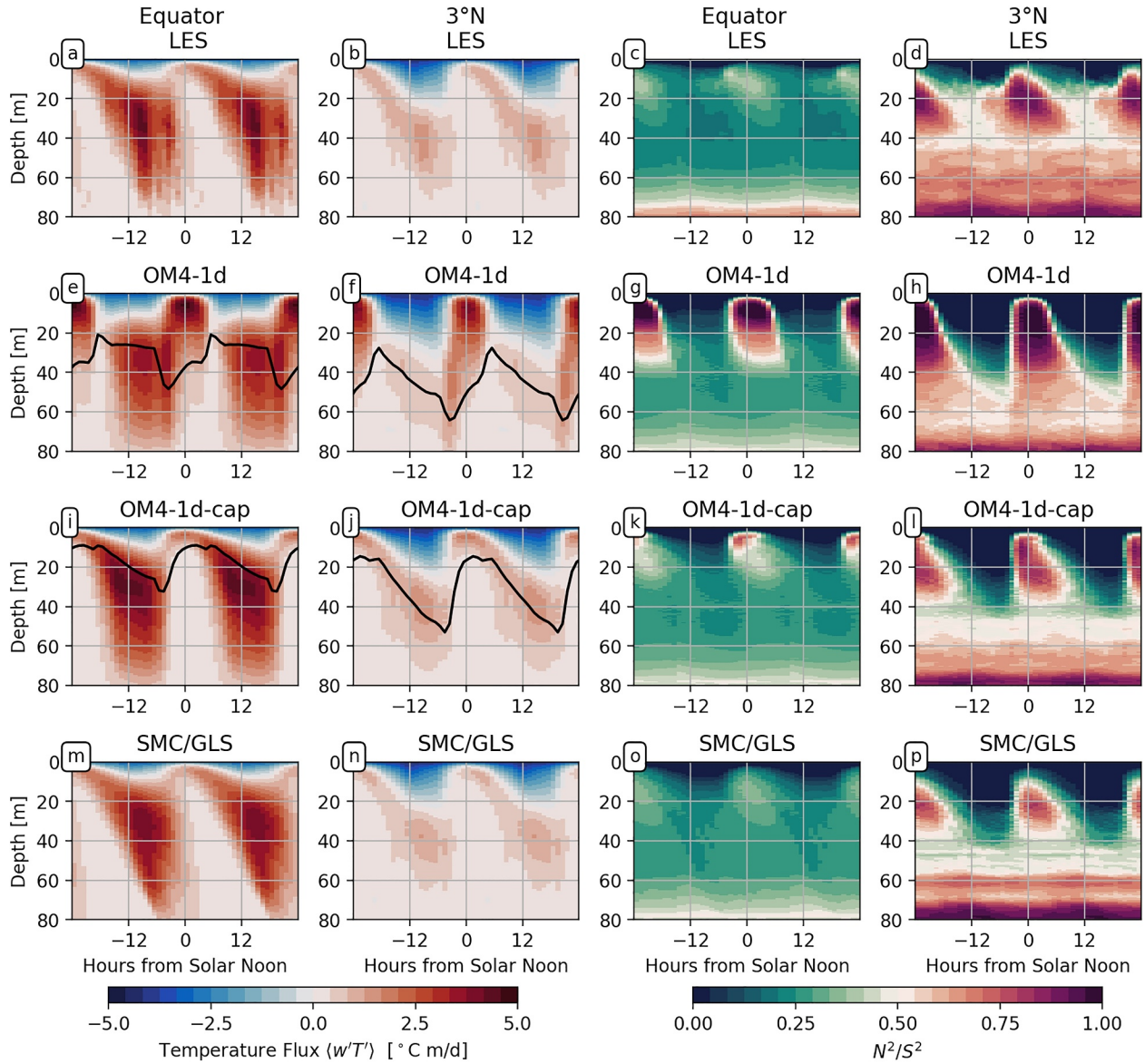

Figure 6. Diurnal composite of large eddy simulation (LES) (1st row), OM4-1d (2nd row), OM4-1d-cap (3rd row), and SMC/GLS (4th row) simulations for vertical turbulent temperature flux (positive downward, first and second column) and gradient Richardson number ($Ri = N^2/S^2$, third and forth column) at 140°W, for the equatorial (first and third column) and 3°N (second and fourth columns) sites. In panels (e, f, i, and j) the black line is the mean value of the ePBL boundary layer depth. For the Richardson number composite averages, the hourly data is capped between zero and one, to avoid skewing the average toward small or large values of Ri. LES provided from Whitt et al. (2022).

these runs mimic the LES (top row) diurnal variability of the temperature flux and the Richardson number, much better than in the original OM4. In particular, the $m_* \leq 1.25$ cap successfully shuts off the overly strong ePBL mixing during the daytime, allowing the JHL scheme to dictate the mixing coefficients. These improvements also result in more high frequency variability in the upper 50 m of the temperature and currents, consistent with the LES (Figure 4 (third column)).

3.2.2. Remaining Difference Between OM4-1d and LES

While the OM4-1d-cap experiment improved aspects of the OM4-1d simulation compared to the original model, there are still aspects of the simulation that do not agree well with the LES. Understanding the rapid deepening of the temperature flux in the OM4 and OM4-1d-cap experiments requires revisiting the theory that underpins the JHL shear mixing scheme. One assumption in developing the set of equations employed by JHL is that the

turbulence develops rapidly compared to the mean flow (e.g., the TKE tendency term is ignored, and a steady-state equation for TKE is solved). This simplification of the dynamics helps the JHL model to be less sensitive to model details like timesteps and vertical resolution, but turns out to be the cause of the overly rapid penetration of the nighttime temperature flux. This feature is demonstrated by comparing the OM4-1d-cap results to a separate one-dimensional model test that uses a second moment closure (SMC). For the SMC we use the Generic Length Scale (GLS, proposed by Umlauf & Burchard, 2003) parameterization that includes a non-equilibrium, prognostic TKE equation as implemented in the General Ocean Turbulence Model (GOTM, gotm.net). In the SMC/GLS simulation, the slower penetration of the vertical temperature flux observed in the LES is recovered by the column model (Figure 6, panels m and n). We verify that the important difference between the SMC/GLS and JHL is the turbulence storage term, by iterating the TKE and length equations in the GLS model 10 times within each model time step, effectively bringing the turbulence in the SMC/GLS to equilibrium as is prescribed in JHL. The too-rapid penetration of the vertical temperature flux in JHL is recovered by SMC/GLS with the equilibrium turbulence, indicating that the adjustment time for the turbulence to the mean state is important for properly simulating these high-frequency characteristics of the turbulent fluxes.

This exercise indicates a role of the TKE adjustment time (storage term) in the vertical temperature flux in deep-cycle turbulence. Further investigation will be undertaken in future research into the simulation in OM4 of the diurnal cycle of turbulence with SMC or an additional TKE storage term in JHL. Future research efforts are needed to implement either approach in global OM4 configurations to modify JHL or to accommodate long time steps with SMC (see Reichl & Hallberg, 2018). We also note that none of the 1d experiments accurately captures the depth of very low ($\leq$0) Richardson number at night, especially at 3°N. Some of this difference is likely related to the strictly down-gradient mixing assumption within all of the vertical mixing schemes employed here. "Down-gradient" vertical fluxes require that the property fluxes are proportional to the oppositely signed vertical property gradient. For example, a positive temperature flux (e.g., negative downward as in the upper 20 m at night at 3°N) must be accompanied by an unstable (negative) vertical temperature gradient (and hence negative N^2). The LES is not constrained to have down-gradient vertical mixing, predicting non-gradient vertical fluxes during nighttime convection. Including non-gradient fluxes in OM4-1d is not investigated further in this work (e.g., see Large et al., 1994).

3.3. Impact of Improved Diurnal Turbulent Fluxes on Stratification and Shear

The diurnal patterns of turbulent mixing and stability indicate that OM4 with the m_* cap can simulate the primary features of vertical mixing in the upper 50 m, including the deep cycle of turbulence. The impact of the OM4-1d-cap experiment on the longer-term (weekly to monthly) evolution of mean temperature and zonal current turns out to be small (compare Figure 4, 3rd column). This weak sensitivity is because the mean heat fluxes into the ocean are largely constrained by the (uncoupled) forcing in these experiments, including surface forcing and imposed large-scale tendency profiles. Thus, the daily mean heat fluxes at a given depth are not significantly different in any experiments, despite the modulation of the diurnal cycle. Instead, the impact of the cap in these experiments is primarily only on higher-frequency (e.g., sub-daily) variability of temperature and currents, especially at the equator.

The improved diurnal variability of the fluxes is reflected in the diurnal anomaly composite (see Figures 7 and 8), defined here by taking the diurnal mean composite and subtracting the time mean at each depth, to reveal the amplitude of the diurnal variability as a function of depth. The phasing of the vertical penetration of relatively warmer and colder water (panels a and b) and more or less eastward flow (panels c and d) is seen to occur gradually in the LES, with the time of the peak temperature and current at the surface preceding the time of the similar peaks at 20 m depth by about 6 hr. In the OM4-1d experiment this phasing is almost instantaneous in time, where the peak values of temperature and currents are nearly coherent in the vertical (panels e and h). This phasing is improved in the experiment with the m_* cap (panels i and l), and the diurnal amplitude of SST is in turn also significantly increased (now too strong). The SMC/GLS predictions of diurnal temperature and current anomalies agree closely with the LES, providing further evidence of their skill in simulating the diurnal evolution of turbulence and its impact on the mean fields (Panels m and p).

The mean fields and turbulence metrics are bridged by looking at the diurnal anomaly of shear and stratification (Figure 8). The OM4-1d-cap simulations are also more consistent with the LES than the original OM4-1d model for simulating the diurnal anomaly of these quantities, especially in the upper 40 m. These are important mean

10.1029/2023EA003485

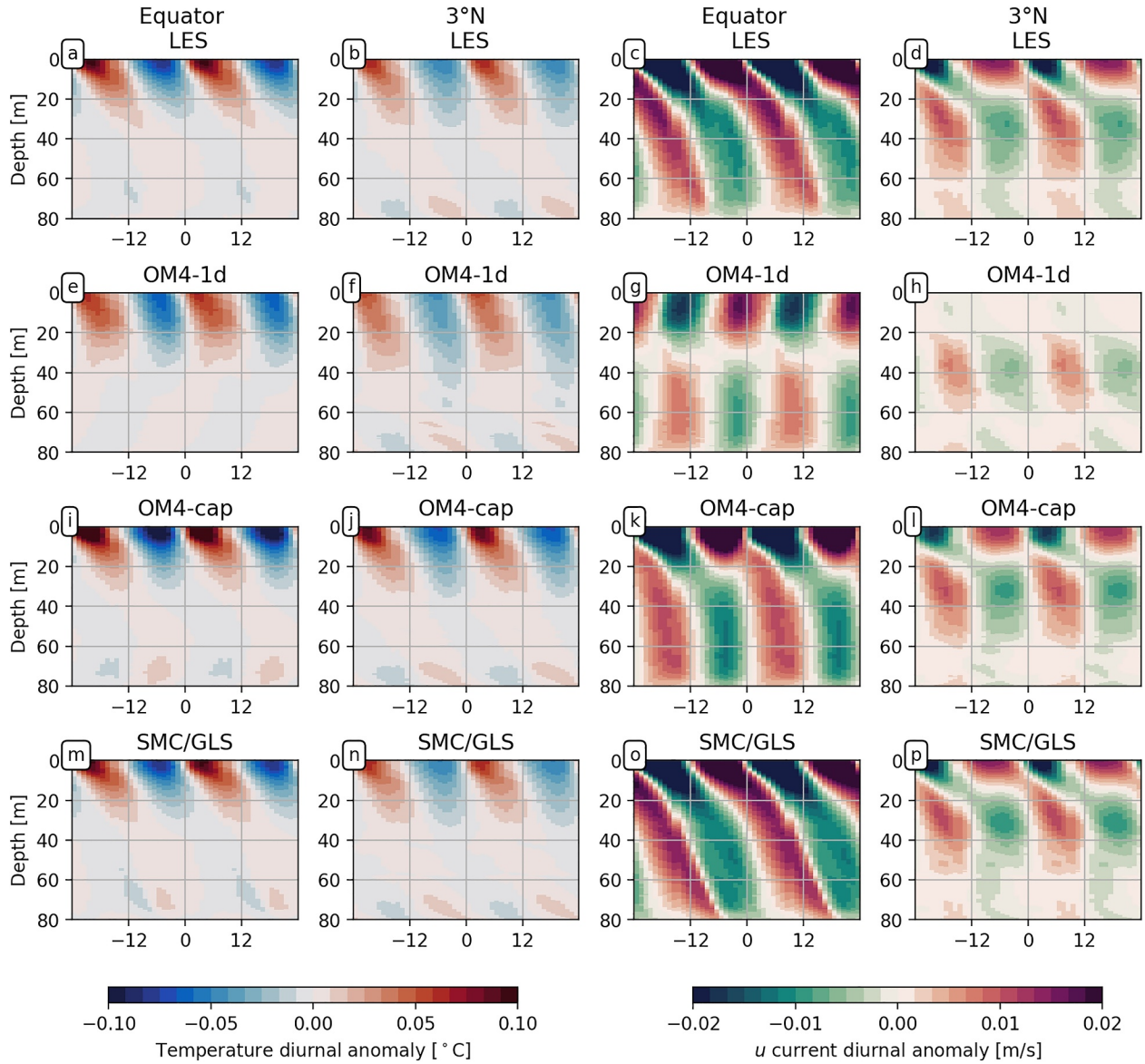

Figure 7. Diurnal composite anomaly, relative to the long-term diurnal mean, for the large eddy simulation (LES) (1st row), OM4-1d (2nd row), OM4-1d-cap (3rd row), and SMC/GLS (4th row) simulations, for temperature (first and second column) and zonal velocity (third and fourth column) at 140°W. Results are shown for the equator (first and third column) and 3°N (second and fourth columns). LES provided from Whitt et al. (2022).

field metrics since the stratification and shear directly couple the mean fields to the turbulence parameterizations. The turbulence metrics derived from the LES (such as vertical heat fluxes) are difficult to estimate routinely from observations outside of a few locations and depths (e.g., Warner & Moum, 2019). These results motivate further analysis of diurnal and longer time-scale variability of the vertical current shear and stratification in OM4, and comparisons to longer term observational depth-time series of these mean fields in the following section.

4. Evaluating and Adjusting Upper Ocean Parameterizations in OM4: An OGCM Approach

The evaluation of OM4-1d against the LES yields confidence in an implementation of improved vertical mixing in OM4 from a process perspective. Establishment of the OM4-cap ePBL $m_* \leq 1.25$ update especially improves the simulation in the upper 80 m equatorial ocean. However, this exercise was conducted within a controlled one-dimensional experiment with prescribed large-scale forcing, including both atmospheric and large-scale oceanic

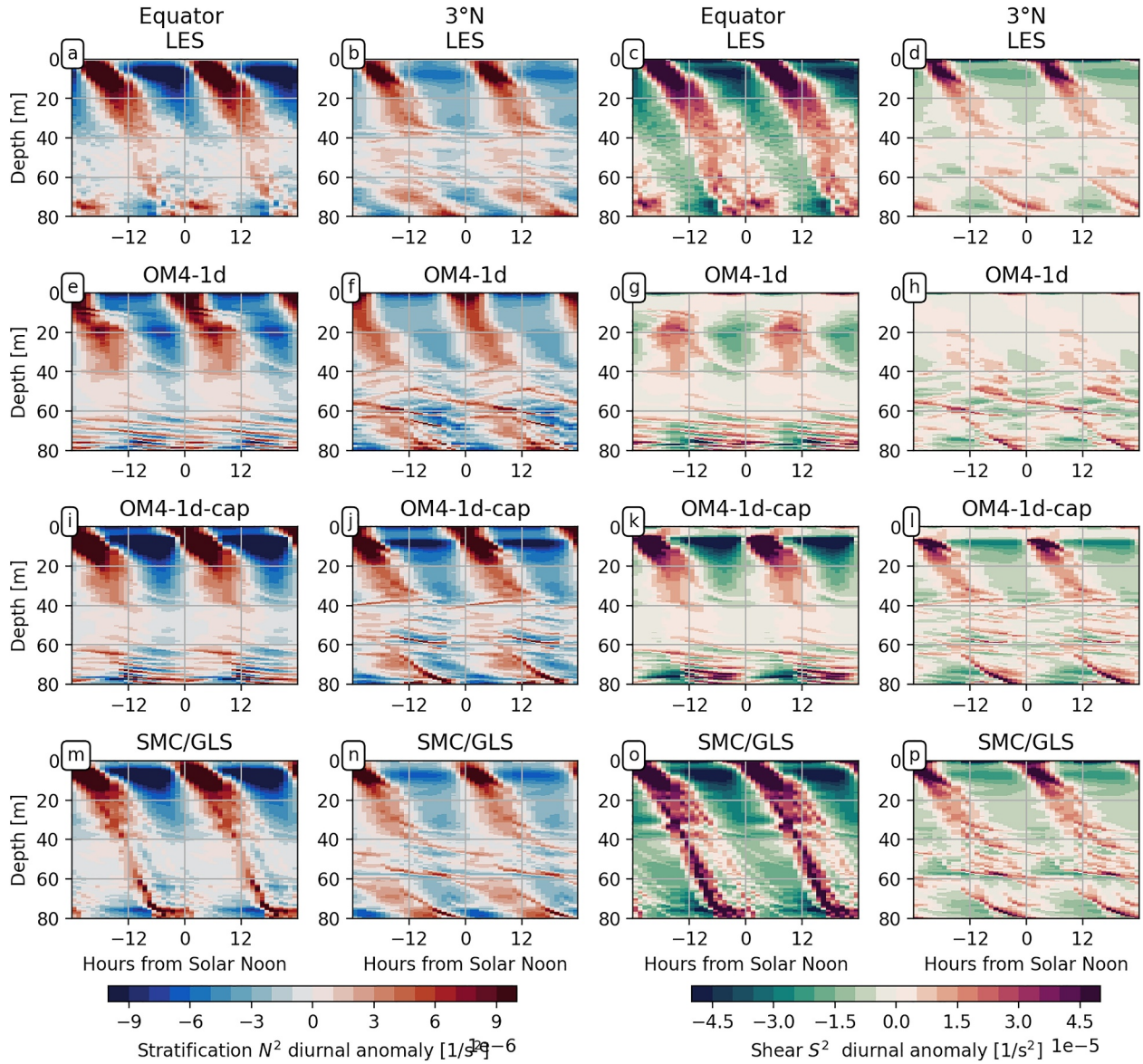

Figure 8. As in seven, but for vertical stratification (N^2, first and second column) and vertical shear (S^2, third and fourth column).

processes. We now present an evaluation of several global OM4z_* experiments (see Section 2.1.3), including the ePBL m_* cap of 1.25, in order to evaluate how the improved representation of vertical mixing impacts the 3d simulation. We focus on testing the impacts of modifications to the OM4 model against long-term observations in the equatorial Pacific Ocean.

4.1. Observational Data Sets

4.1.1. TAO Mooring Measurements of Currents and Density

The long term, high-frequency nature of the observations taken along the Tropical Atmosphere Ocean (TAO) mooring array provides a useful database to assess the mean and variability of currents, current shear, density, and stratification in OM4. We therefore compare high-frequency profile outputs taken from OM4z_* runs to four TAO moorings (165°E, 170°W, 140°W, and 110°W) with long-term ADCP (acoustic Doppler current profiler) records in the equatorial Pacific. We utilize estimates of the zonal and meridional 2-hourly mean currents from the ADCP

in 5 m bins from roughly 50–250 m depth. These current measurements can then be used to estimate the vertical current shear and its diurnal variability.

The four TAO mooring locations in this analysis also include some sensor recordings of temperature and salinity within the upper ocean. During the 2000–2020 time period, the temperature sensors were typically limited to 10–15 discrete measurements throughout the upper 200 m at these four locations (except a few periods of more intense observations, e.g. as in Masich et al. (2021)). The salinity measurements are even more limited, often including only about seven measurements in the upper 125 m and only for a few years since 2015. Despite the limited vertical resolution of the observations, they provide hourly (or finer) measurements of density that are useful to infer stratification variability ranging from subdiurnal to inter-annual timescales.

In all analyses we use properties on depth surfaces. Projecting the currents and gradients into density space would reduce the noise ascribed to isopycnal heaving. Yet due to the coarse vertical resolution of the TAO density data, we do not pursue transformations into density coordinates.

4.1.2. Argo Based Stratification

To supplement the relatively low vertical resolution TAO-based estimates of stratification, we also diagnose stratification from Argo profiles (Argo, 2023). The Argo floats usually report temperature and salinity at a vertical spacing of roughly 1−4 m throughout the upper 2,000 m of the water column, and offer continuous coverage since 2004. Individual Argo profiles can take several hours to complete, and may not be repeated in a similar location for several weeks or even months, making it difficult to infer shorter time variability in density and stratification. We therefore use Argo to infer detail about the vertical structure of stratification and its variability, especially at monthly and longer timescales. The Argo data effectively represent something close to a snapshot in time, since the floats usually ascend/descend about 2–3 m per minute. To make the Argo statistics more compatible with the 2-hour time-averaging that we apply to the TAO and OM4 data, we also remap Argo data onto the vertically coarser OM4 z_* grid (see Figure 1). The lack of time averaging beyond a few minutes in Argo means some high-frequency variability can remain, but the coarsening filters out high wavenumber vertical variability with scales less than the OM4 vertical grid spacing. The model is still not expected to capture all details of the high-frequency variability of stratification observed by Argo.

We locate Argo profiles within ±0.25° of the equator in latitude, and within ±5° of the station in longitude, yielding between 650 and 750 individual profiles per location. The aspect ratio of the sampling box allows us to obtain additional profile matches, and reflects that the zonal scale of the EUC and thermocline variability is much wider than its meridional scale.

4.1.3. Mean Properties and Percentile Distributions From Observations

We first show the mean fields and their statistical distributions, as measured by the TAO and Argo instruments (Figure 9). The gray shading in the figures indicates the distribution percentiles for the 2-hourly time series (from TAO) and profile data sets (from Argo) at each depth, for the zonal current, vertical shear of the horizontal current, surface referenced potential density, and vertical density stratification from the data. The darkest black shading represents the median (50th percentile) values. The smaller and larger percentiles indicate the distribution (envelope) of the observed values at each depth.

The range of observed currents is typically bounded between about −1 and 1.5 m s^{-1}, with significant variability at all sites and significant structure in the mean current profile (Figure 9 top row). The percentile maps yield insight into the typical EUC zonal flow, and variability of its depth and strength as it flows from west to east. We also plot the percentile shaded maps for the squared vertical shear of the horizontal current components computed from the 2-hourly mean ADCP data (Figure 9, panels e–h). The shear shows typically much higher values occurring above the mean position of the EUC core (i.e., the position of the peak positive values in the zonal current, u), with a kink indicating lower values of mean shear within and below the EUC core. The percentile maps suggest considerable variability in the current shear, which may be related to seasonality, large-scale current variability (such as TIWs, meridional meanders of the EUC, equatorial Kelvin waves, and ENSO), and higher-frequency processes such as deep cycle turbulence and internal waves. The shear is roughly log-normally distributed, so we also plot the mean which is skewed toward the largest values.

10.1029/2023EA003485

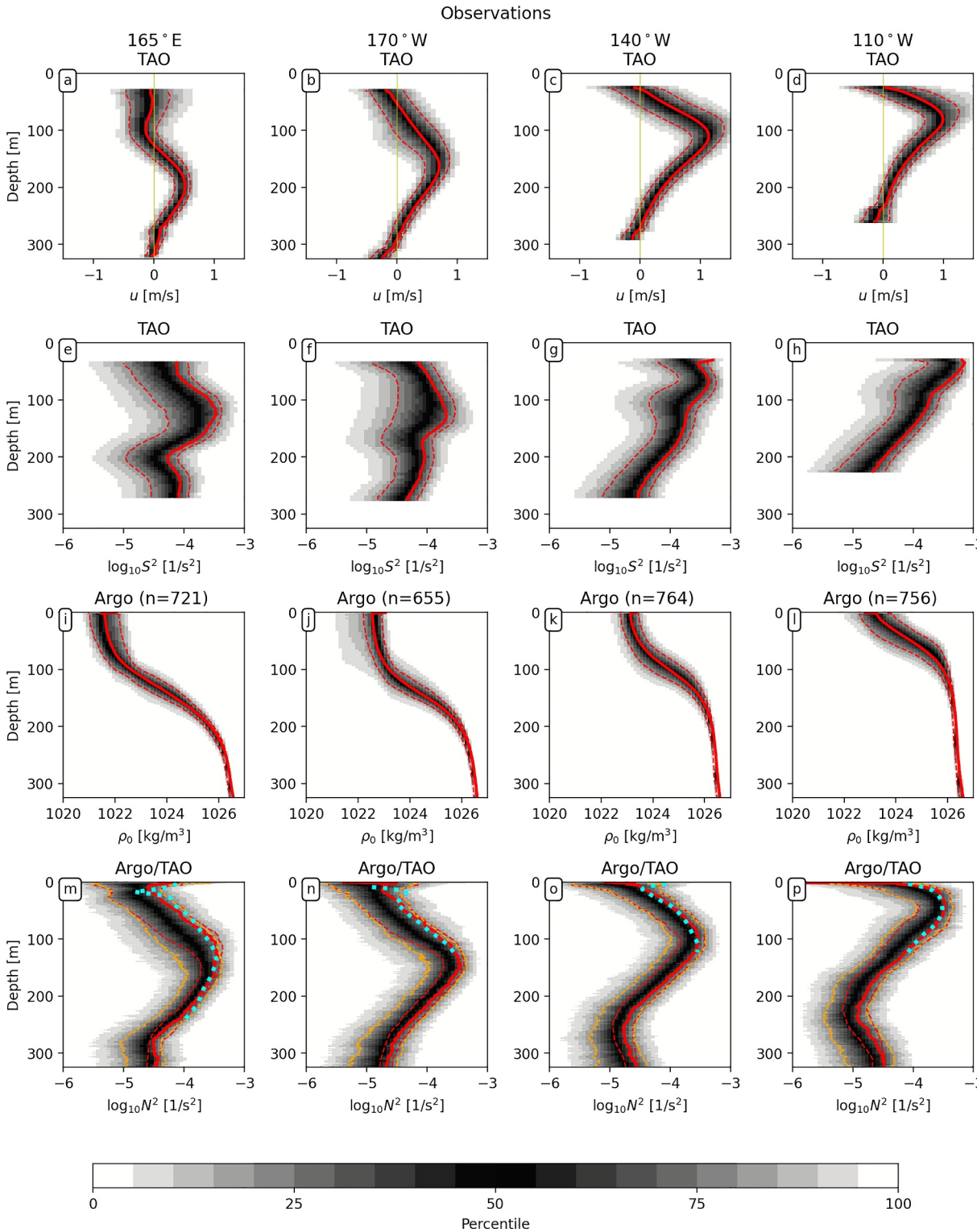

Figure 9. Percentile corresponding to each abscissa value, along each depth on the ordinate, for the zonal current (upper row), squared vertical shear of total horizontal current (second row, note the log scale), potential density (third row), and density stratification (bottom row, note the log scale). The columns span the equatorial Pacific from 165°E to 110°W. The dashed red lines show the 20th and 80th percentiles, and the solid red line shows the mean. In the bottom row, the 20th and 80th percentiles are computed both using full recorded resolution (orange) and after coarsening the density to the vertical grid of OM4 (red, see Figure 1). The tropical atmosphere ocean (TAO) derived mean stratification is also shown in cyan for comparison. TAO data covers the years from 2001 to 2008, while the Argo data includes the full Argo time period (through 2022) to increase the number of samples (indicated by n in panels i–l).

From the Argo profiles we compute the potential density profile and its distribution (Figure 9, panels i–l). The profiles show a clear shoaling of the pycnocline toward the east, roughly coinciding with the shoaling of the EUC, and fairly large variability of the density within and above the pycnocline. Variability of the pycnocline depth is linked to heaving at subseasonal to inter-annual timescales, due to equatorial Kelvin waves and wind pattern shifts associated with the seasonal cycle and ENSO.

We apply the Argo diagnosed density to estimate the stratification and its variability in Figure 9 (panels m–p). The stratification is roughly log-normally distributed; again we plot the mean, which is skewed toward the larger values. Stratification variability estimated from the Argo profiles shows significant variations within and above the pycnocline. In the far west, the peak mean stratification near 150 m (panel m) occurs above the shear minimum near 200 m (panel e). However, farther east there is a closer correspondence between the typical depths of the local shear minima and stratification maxima (particularly near 100 m depth at 140°W, panels g and o). We also compare the TAO and Argo estimates of the stratification bulk statistics, and find that they are mostly consistent — supporting the notion that the two can supplement one another.

4.2. Comparison to OM4z_*-Cap With $m_* \leq 1.25$

We now evaluate the OM4z_* experiments against the TAO and Argo observations, to understand the impact of the m_* cap in the full-complexity global model. The model cannot simulate motions with horizontal scales less than about 50–100 km and vertical scales less than about 4 m, so it cannot capture all variability due to all processes captured by the mooring. For example, the models will not capture tides, the full internal gravity wave spectrum, and small-scale instabilities, such as Kelvin Helmholtz type shear instabilities for example, Moum et al. (2011); Smyth et al. (2011).

We now show the 20th–80th percentile ranges of the OM4z_* 2-hourly output (Figure 10, olive) compared to those for the 2-hourly TAO measurements and Argo snapshots presented in Figure 9. This figure confirms that the global model configuration exhibits many of the same biases seen in the 1d model experiments. For example, OM4z_* produces too little shear throughout the top 300 m of the upper ocean along the equator (panels e–h; note that shear is not observed above 50 m), and too little stratification in the top 20 m (panels m–p). The mean values for the OM4z_*-cap model (orange) indicate that the m_* cap strengthens the shear and stratification in the top 25 m — much as in the 1d model (Figure 8) — but otherwise has little impact on the time mean.

4.2.1. Diurnal Anomalies in OM4 and TAO Mooring Data

Figure 11 evaluates the diurnal anomalies of current shear, comparing the TAO ADCP measurements (panels a–d) against the OM4z_* model (panels e–h) and the OM4z_*-cap model with the m_* cap (panels i–l). The ADCP observations do not extend to the surface, but their climatological diurnal anomalies at 140°W generally match the phasing from the single month LES case study in Figure 8. The OM4 simulations show biases in the shear anomaly in the top 50 m, which appear to be reduced in the OM4z_*-cap experiment, notably at 140°W. Yet there are also substantial vertically coherent signals in the ADCP diurnal shear anomaly throughout the upper 200 m across the basin, which are not simulated in either OM4z_* or OM4z_*-cap.

We also compare the diurnal anomalies of stratification from the TAO moorings (Figure 12) with the OM4z_* models. The TAO temperature and salinity measurements extend close to the surface, enabling us to evaluate the diurnal cycle of stratification in OM4z_*-cap over the top 50 m. The near-surface diurnal cycle in OM4 (panels e–h) is strengthened and improved in OM4z_*-cap (panels i–l), consistent with reduced vertical mixing during the day as seen in the 1d models. Interestingly, the observations show diurnal variations of the stratification within the upper pycnocline that are not reproduced in any of the models. These observations suggest that the diurnal cycles of turbulence and mixing might well penetrate into the stronger stratification found at depth; however, these aspects are not simulated by either OM4z_* or OM4z_*-cap.

4.2.2. Monthly Variability in OM4 and TAO Mooring Data

The TAO and Argo records also provide insight into longer timescale variability. We next investigate this variability by showing the monthly climatology for shear (Figure 13) and stratification (Figure 14 shown for TAO, the Argo results are consistent). These results suggest relatively little impact of the improved diurnal cycle mixing in OM4z_*-cap on the climatology in ocean-only mode, also consistent with the result in the LES

10.1029/2023EA003485

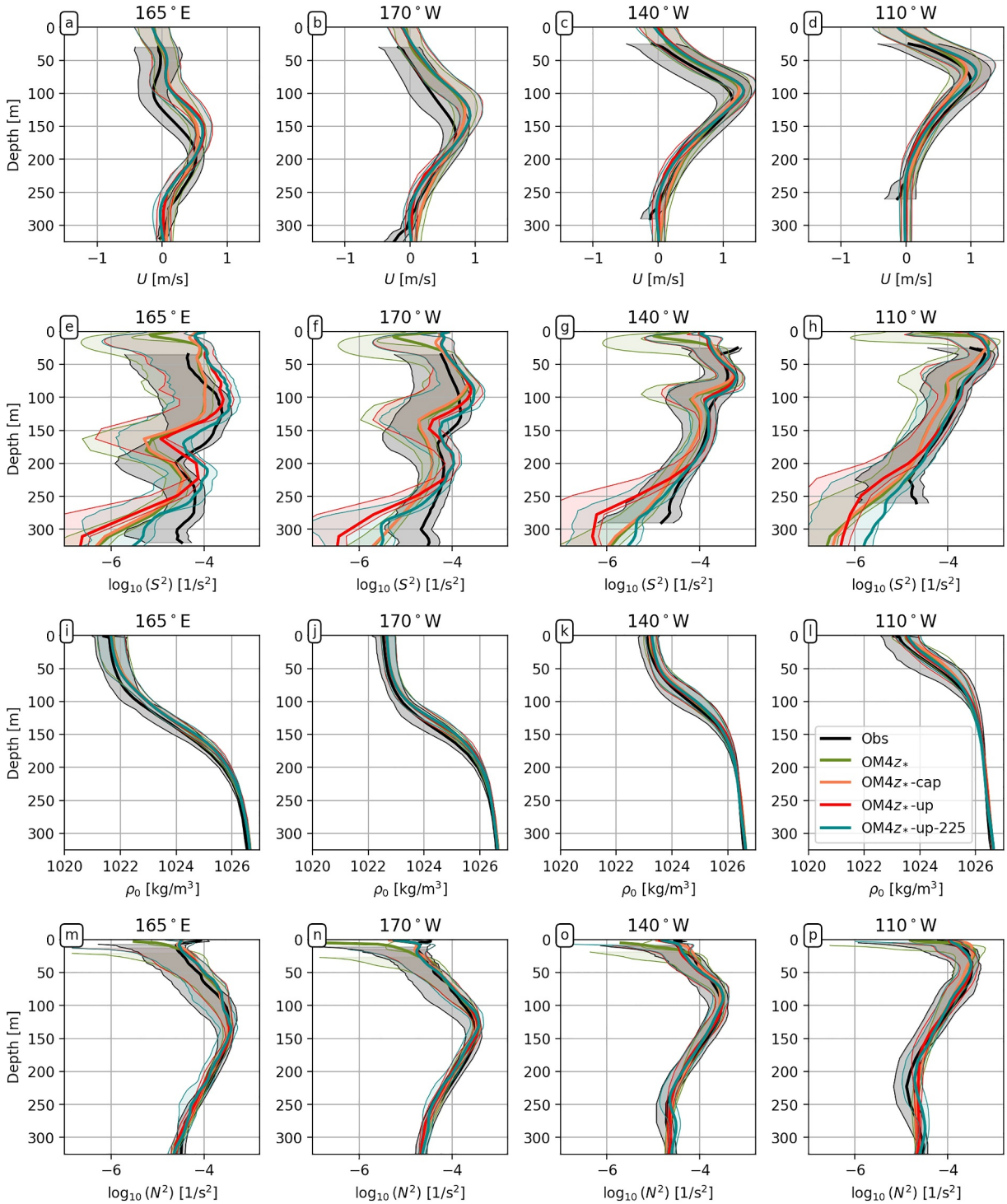

Figure 10. Comparison of the 20th and 80th percentile (thin lines) and mean (thick line) profiles from OM4 and the observations presented in Figure 9. Black curves with shading represent observations. The corresponding olive curves are for the 75-level OM4z_* simulations using the original settings. Orange curve shows the mean of OM4z_*-cap (percentile curves are hidden to reduce clutter). Red curves represent the OM4z_*-up model, with all updates discussed in this manuscript. Teal curves are for the 225-level version of OM4z_*-up.

comparison. The primary differences that arise upon close examination are within the upper 25 m in both figures (panels e–h vs. panels i–l), where OM4z_*-cap produces stronger shear and stratification than OM4z_*. The OM4z_*-cap model shows several key differences from the ADCP shear, especially the lack of a high shear region between

10.1029/2023EA003485

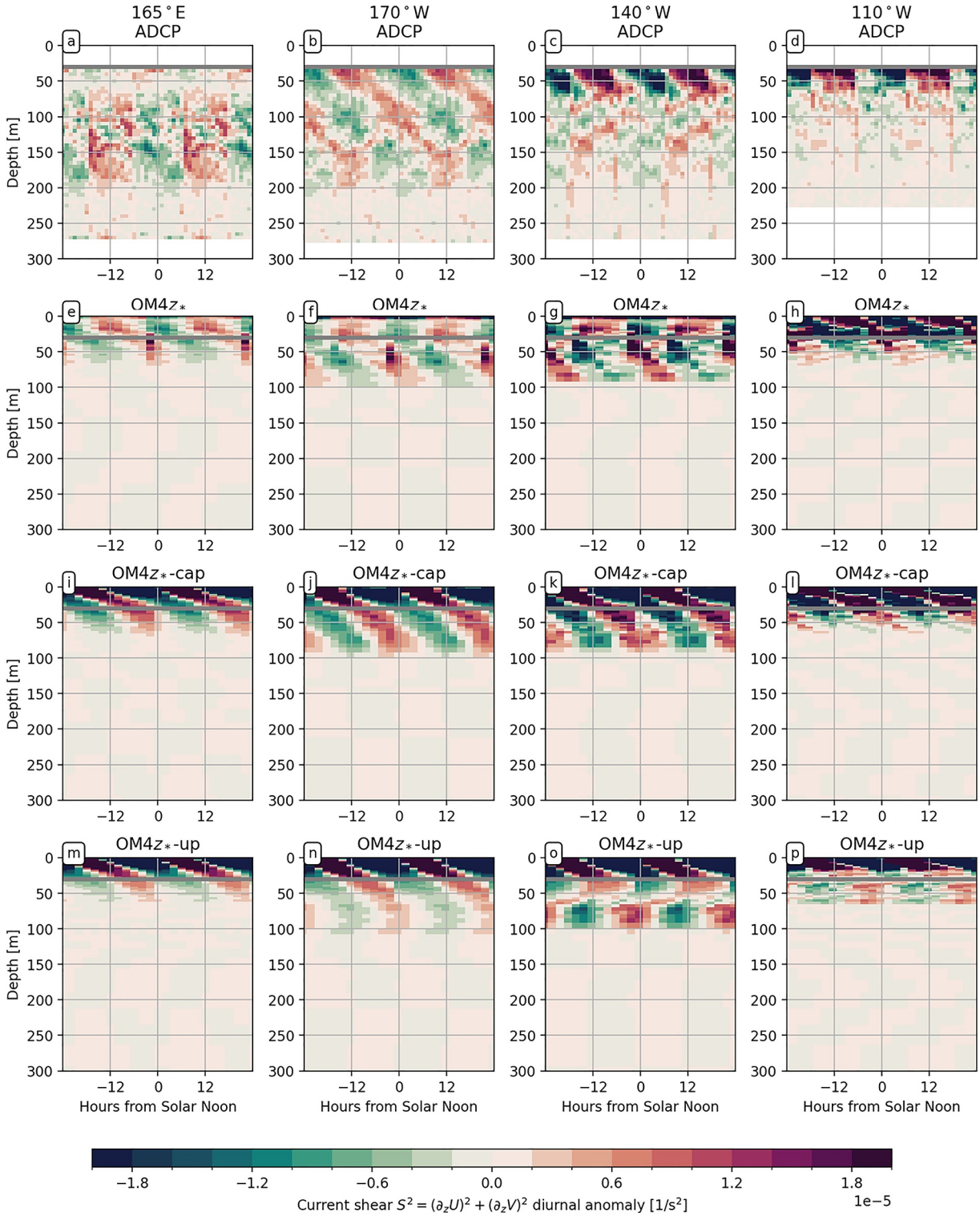

Figure 11. Diurnal anomaly of total vertical current shear squared (S^2), at four Pacific tropical atmosphere ocean mooring locations along the equator (columns). Top row is from acoustic doppler current profiler observations. Second row is the OM4 z_* experiment. Third row is the OM4 experiment with the ePBL m_* cap. Fourth row is the OM4 experiment with all updates discussed in this paper.

10.1029/2023EA003485

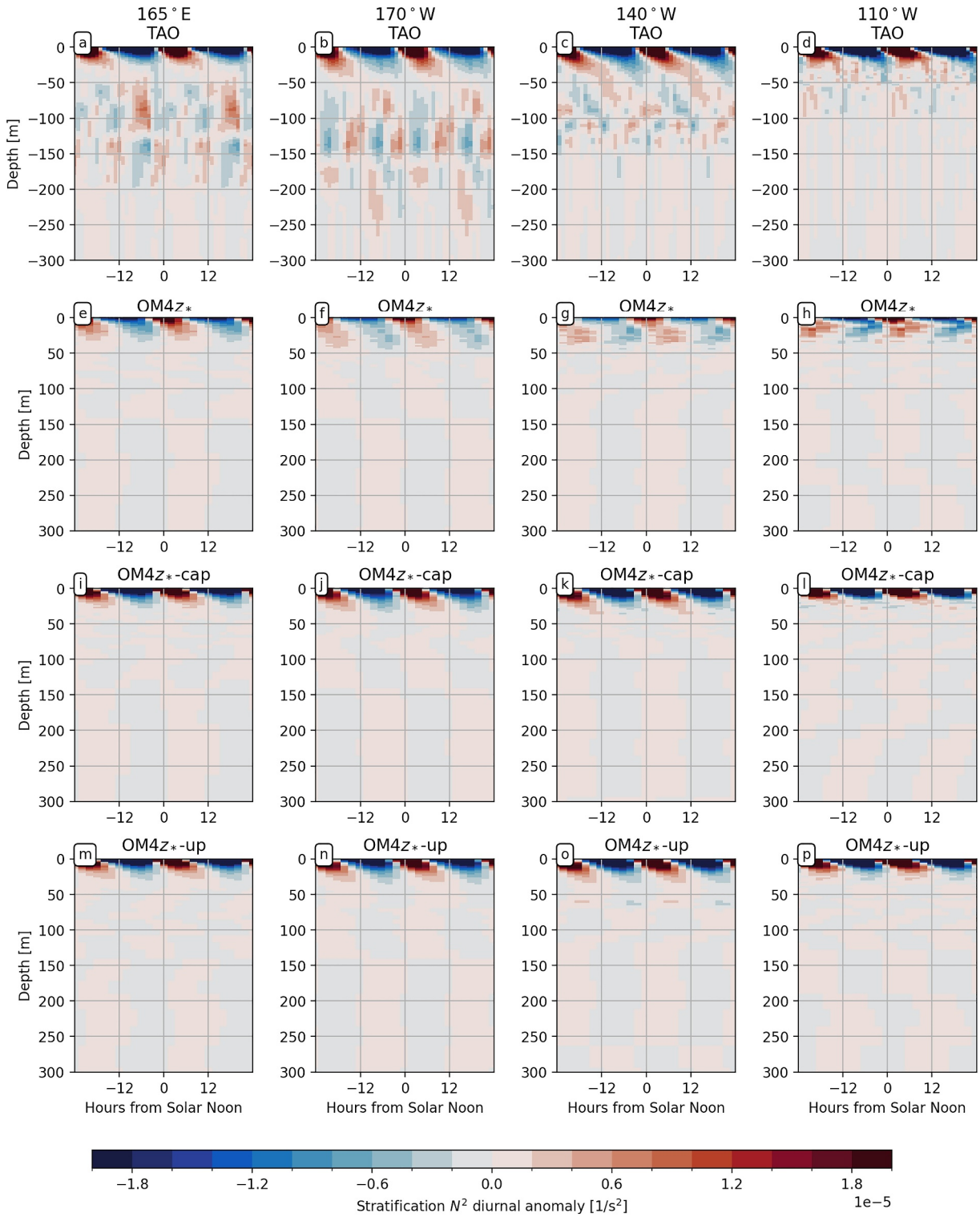

Figure 12. Diurnal anomaly of stratification (N^2), at four Pacific tropical atmosphere ocean (TAO) mooring locations along the equator (columns). Top row is computed from TAO temperature and salinity observations. Second row is the OM4 z_* experiment. Third row is the OM4 experiment with the ePBL m_* cap. Fourth row is the OM4 experiment with all updates discussed in this paper.

10.1029/2023EA003485

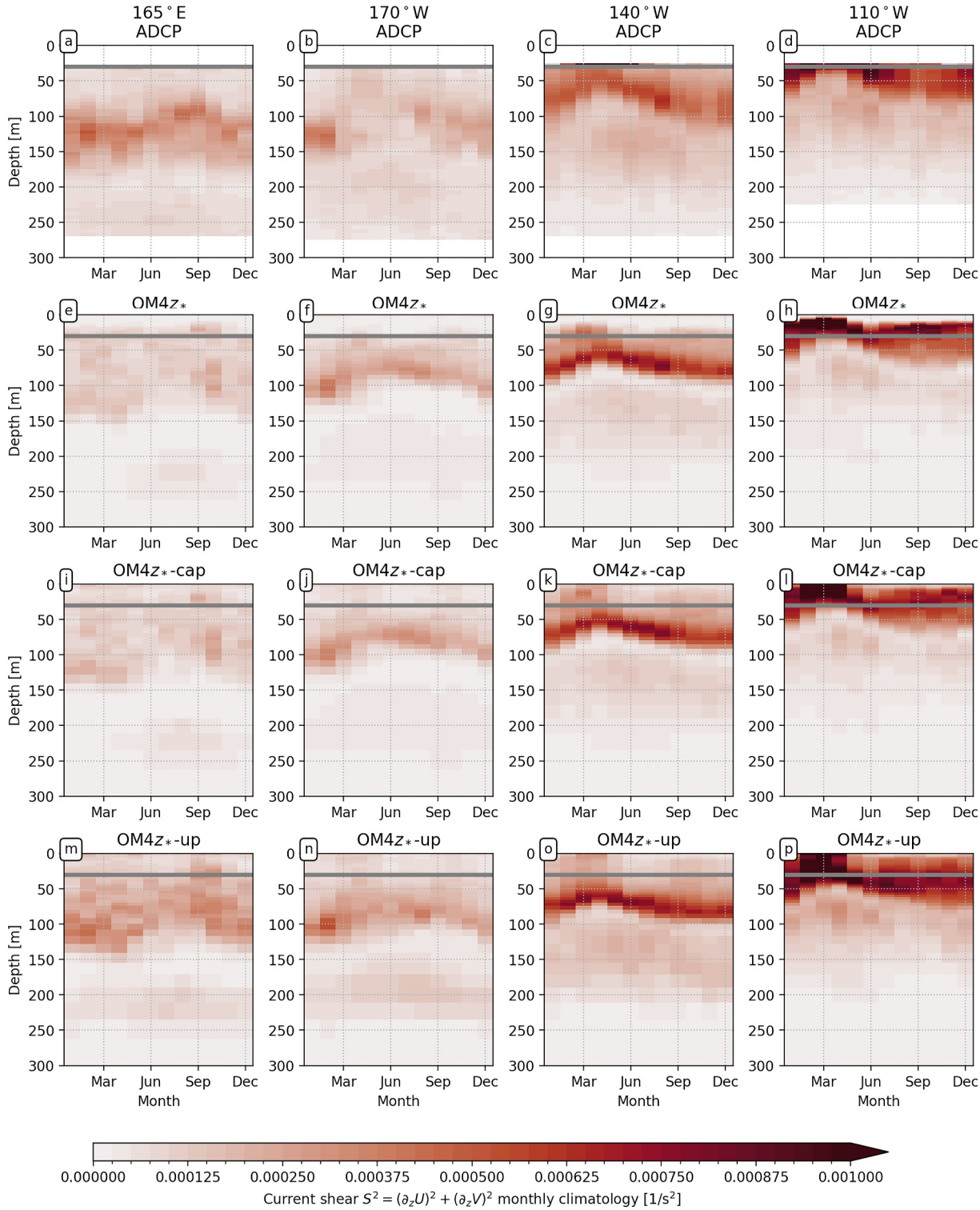

Figure 13. As in Figure 11, but for the monthly climatology of total vertical current shear squared (S^2).

100 and 150 m at 165°E, and the lack of significant shears below the EUC core at all four sites. At 110°W, the model's excessive stratification in the top 25 m (similar to that noted in Figure 3) is not improved by the m_* cap (compare Figure 14, panels d, h, and l). We simulated the full OM4 OMIP2 simulation with the m_* cap

10.1029/2023EA003485

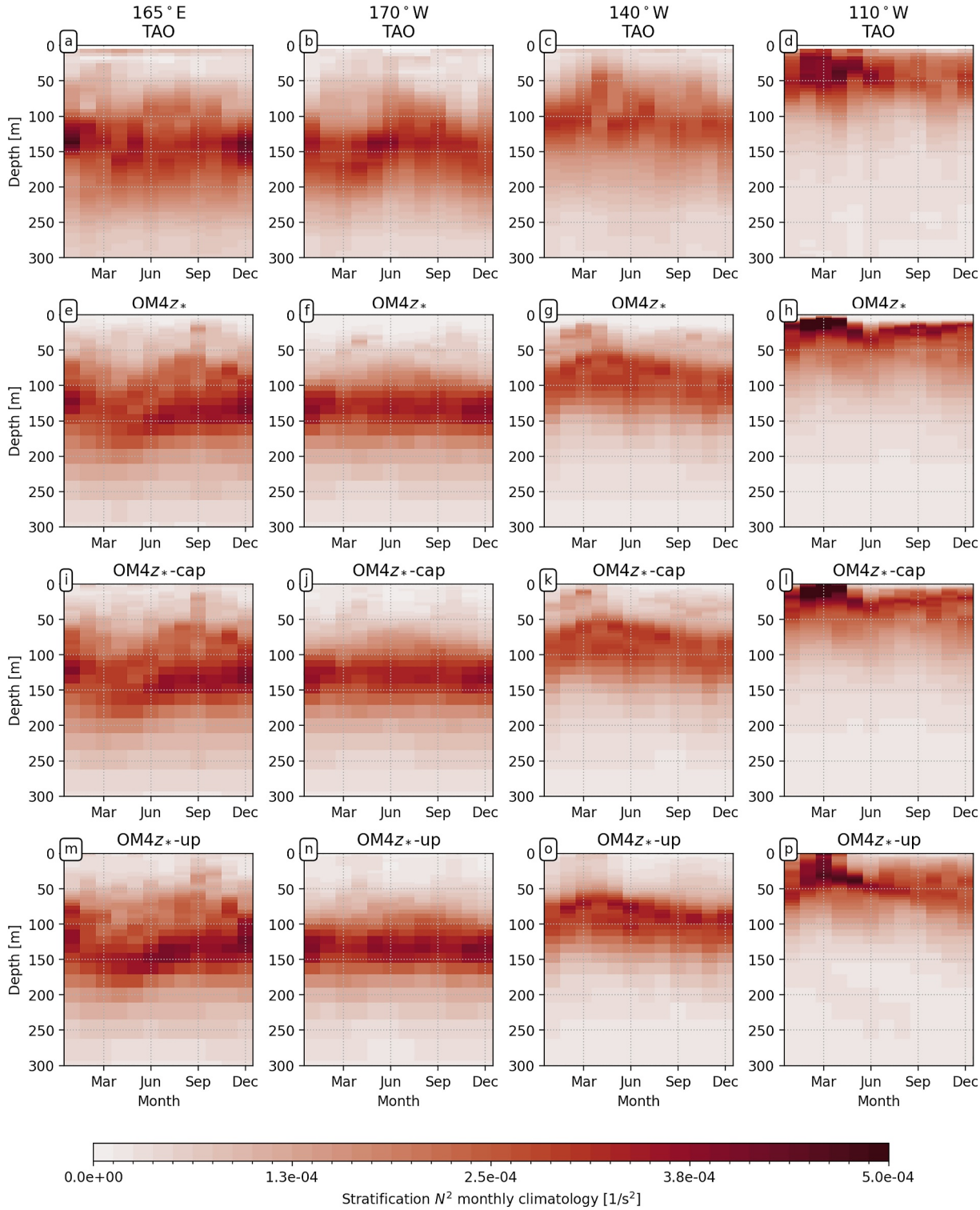

Figure 14. As in Figure 12, but for the monthly climatology of stratification N^2.

configuration to reproduce Figure 3 and compare, and saw no evidence of any improvements in the long-term solution. In Section 4.3 we therefore explore other possible causes of OM4's shear and stratification biases, focusing on processes not tested in the LES comparison that could impact the mixing deeper in the water column.

4.3. Additional OM4 Modifications

The comparisons with LES and observations support the capping of m_* in the upper 50 m in OM4, and indicate that the OM4 1-d simulations can generate reasonable profiles of vertical mixing when the background fields are constrained as in the LES. The LES does not capture all processes that can drive mixing in the ocean, since, for example, it only captures processes that it can resolve and that are forced by its imposed boundary conditions. We next explore other model choices for representing uncertain processes, to better understand the remaining biases below 50 m. We ran several dozen additional configurations of OM4 and analyzed how the results compared to OM4 and OM4-cap. The experiments included varying many uncertain OM4 parameters, such as the shortwave solar penetration, MLE restratification, numerical implementation choices of JHL shear mixing, and other mixing choices. From these tests, we identified two additional choices for the ocean mixing parameterizations that have particular influence on the tropical ocean biases.

The first of these is the addition of a new choice for computing the JHL mixing coefficients (parameter setting "VERTEX_SHEAR = True" in MOM6), where the model temperature, salinity, and currents are interpolated to the horizontal C-grid cell vertices instead of the default of interpolating the currents to the C-grid cell centers. A large motivation for this change is to avoid checkerboard patterns in the mean fields related to numerical noise issues that traditionally plague Richardson number based mixing schemes. The second change is to disable the large background viscosity of 10^{-4} m^2 s^{-1}, which (given an assumed Prandtl number of 1) sets the background vertical viscosity equal to the background tracer diffusivity of 2×10^{-6} m^2 (Harrison & Hallberg, 2008) at the equator. The high viscosity setting had persisted in OM4 despite having no physical justification, perhaps related to historical reasons that are no longer necessary in MOM6.

We examined the impact of these two modifications separately (not shown). While the vertex shear choice helps to mitigate grid scale noise, it has little impact on the time mean stratification near the equator. However, removing the background viscosity has a large impact on the zonal shear, especially at the eastern mooring site (110°W): it leads to a less diffuse mean EUC, with stronger vertical shear, lower Ri, and increased vertical diffusivity from the JHL parameterization. The enhanced diffusivity leads to better large scale mean stratification compared to the original OM4. We conducted sensitivity tests and found a similar impact by reducing the background viscosity to any value below 10^{-5} m^2 s^{-1} instead of setting it to zero, but are otherwise unable to constrain its precise value in these experiments.

We present results that analyze the three OM4 updates together, including the $m_* \leq 1.25$ cap, the updated JHL shear mixing scheme, and the reduced background viscosity. This version of OM4z_*, denoted OM4z_*-up for the remainder of this manuscript, yields many improvements. The one-dimensional model results presented in Section 3 are not affected by the high background viscosity. This is because the strong parameterized deep cycle turbulent mixing dominates in the upper 60 m and because the EUC shear is imposed in those experiments.

4.3.1. Impact of OM4z_*-Up on Diurnal and Seasonal Variability of Shear and Stratification

We first compare the OM4z_*-up diurnal anomalies of shear (Figure 11, panels m–p) and stratification (Figure 12, panels m–p). At most of the TAO sites the impacts are minimal, and it is difficult to draw conclusions from the comparison with the mooring data (e.g., some shift of the phasing between 50 and 100 m at 170° and 140°W). However, the monthly shear climatology (Figure 13, panels m–p) and monthly stratification climatology (Figure 14, panels m–p) both reveal improvements relative to both OM4z_* and OM4z_*-cap. For example, the OM4z_*-up model has stronger shear below 100 m throughout the basin and throughout the seasonal cycle. We next draw attention to the results at 110°W, where the OM4 and OM4z_* models had a notable strong stratification bias near the surface. The OM4z_*-up model has a much more diffuse (and deeper) pycnocline, especially near the months of September–December, which appears more consistent with observations.

To summarize the improvements, we also show the 20th–80th percentile distribution of the OM4z_*-up model (Figure 10, red) compared to the TAO/Argo observations (Figure 9), the original OM4z_* model (olive), and the OM4z_*-cap model (orange). We specifically note significant improvements of the 50–200 m shear, which reflects the impact of the reduced background viscosity. The peak strength of the EUC in its eastern extent is also better captured, mainly because the reduced vertical viscosity in OM4z_*-up reduces the vertical diffusion of the EUC. Better capturing the EUC and its shear in OM4z_*-up then enables the JHL shear-based parameterization to better

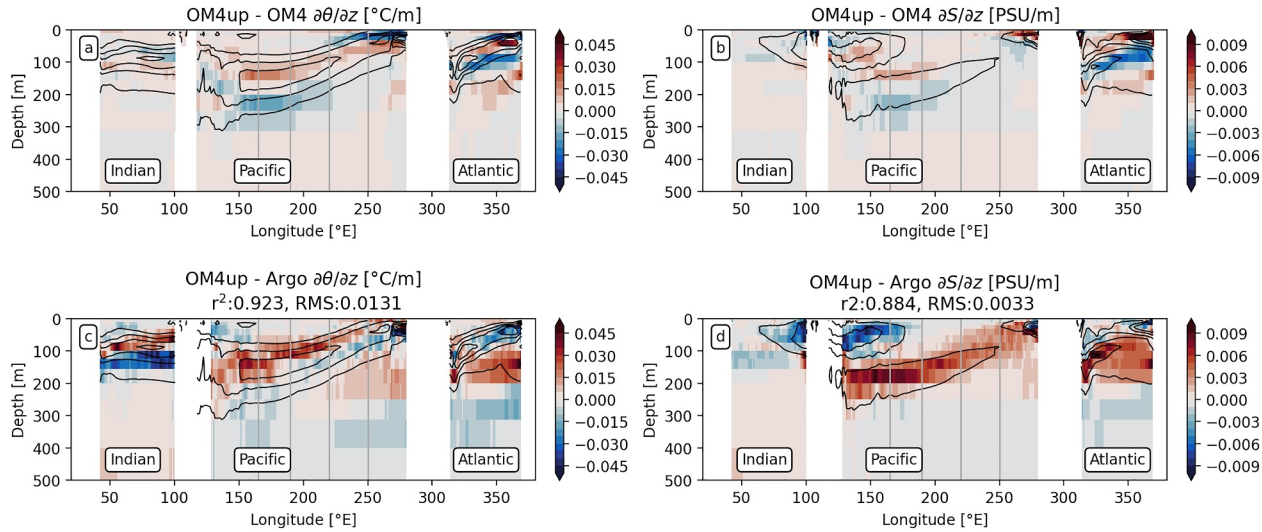

Figure 15. Difference of OM4-up from OM4 for climatological vertical derivatives of potential temperature (panel a) and practical salinity (panel b) and the respective difference of OM4-up minus Argo climatology (panels c and d), all averaged from 1°S to 1°N. The panel titles for the Argo bias maps include the r^2 (Pearson correlation coefficient squared) and RMSD (square root of the mean square difference) difference metrics. The contour intervals in each panel are mapped from OM4-up via interpolation at the same intervals used in Figure 3 to facilitate comparison. The vertical lines indicate mooring locations at 165°E, 170°W, 140°W, and 110°W, which are discussed in Section 4.

predict the vertical mixing. Other biases in the simulation are not improved, including the shallow-EUC bias that may even be worsened at the western mooring sites.

4.3.2. Impact of OM4-Up on OM4 Biases

Figure 15 compares the mean temperature stratification biases between the full OMIP2 simulations of OM4-up and OM4. The shallow stratification biases in the shallow eastern Pacific and Atlantic basins are mostly eliminated in OM4-up, suggesting that the equatorial Atlantic simulation had been suffering from similar issues as in the Pacific. The r^2 over the region improves from 0.88 in OM4 to 0.92 in OM4-up (compared to 0.86 in OM4-cap) and RMSE improves from 0.017 to 0.013°C/m (compared to 0.018°C/m in OM4-cap). We also see slight changes in salinity stratification, with r^2 marginally improving from 0.879 to 0.884 (compared to 0.846 in OM4-cap) and RMSE improving from 0.0045 to 0.0033 PSU/m (compared to 0.0050 PSU/m in OM4-cap). We see that shallow stratification biases in the western basins remain in OM4-up, perhaps even being degraded relative to OM4 at 165°E and 170°W (as was seen in the EUC itself). This shoaling of the EUC in the west suggests that the elevated viscosity may have potentially helped deepen the western EUC (and its associated mixing) toward observed depths in OM4. We do not yet understand the mechanisms that would drive enhanced viscosity in the west, so do not propose enhanced viscosity in this region until further research is conducted to understand the physical processes. It is also possible that the thermocline depth bias in this region can be driven from other non-local sources, for example, a bias in the JRA55-do forcing fields could drive a bias in the large-scale thermocline tilt.

Finally, we note that the improvements in temperature and salinity stratification are reflected in the mean fields as well, with the RMS difference in temperature improving from 0.73°C in OM4 to 0.68°C in OM4-up, and in salinity improving from 0.26 PSU in OM4 to 0.23 PSU in OM4-up (Figure 16). These results suggest that while the LES results led to an improved diurnal cycle in OM4-cap, reducing the vertical viscosity was the main factor in reducing OM4's excessive near-surface stratification in the eastern equatorial Pacific. This high background viscosity was degrading the currents and shears that feed into the JHL mixing parameterization.

We evaluated the OM4-up changes for any potential major impacts outside of the equatorial region, and did not find any significant model degradation. The impacts may be limited to the equatorial region, where the Coriolis parameter vanishes and the dominant dynamical balance is thus between vertical friction and lateral pressure gradients — in contrast to farther from the equator, where geostrophic balance tends to hold. The m_* cap in ePBL

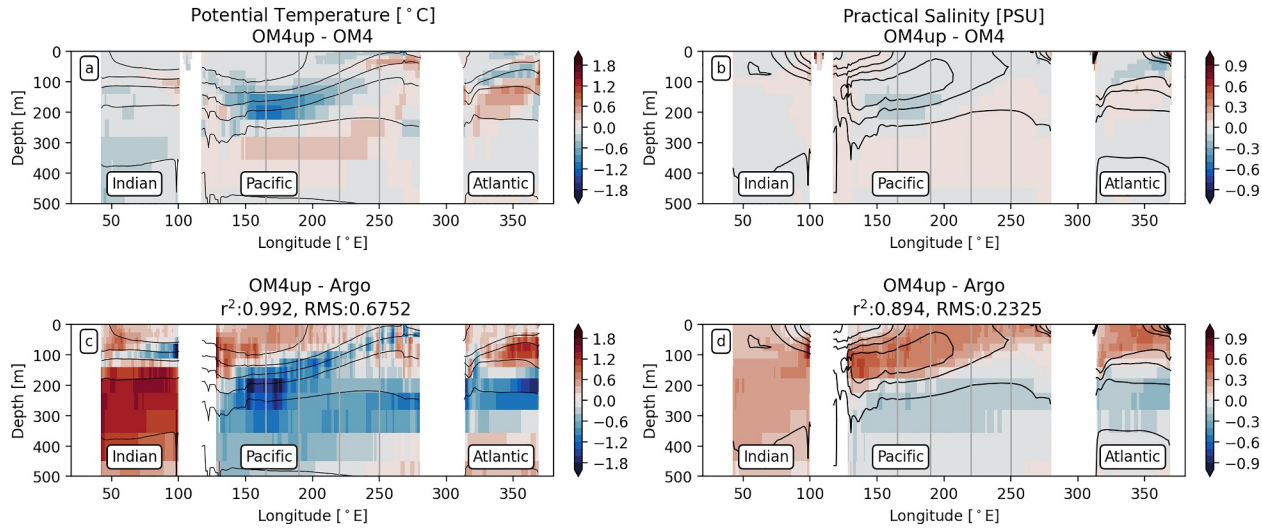

Figure 16. As in Figure 15, but for the potential temperature and practical salinity.

does shoal (worsen) the tropical mixed layer depths by a few percent (not shown), which further motivates future work for a more physically justified fix.

5. Remaining Sources of Bias and the Role of Vertical Resolution

While the choices implemented in OM4-up lead to an improved near-equatorial ocean climate and diurnal cycle relative to OM4, significant work remains to completely address the tropical mixing, thermocline, and stratification biases. We now ask the question, what potential issues may drive the remaining biases?

One candidate is the remaining diurnal phase difference in vertical heat fluxes between OM4-cap and the SMC/GLS vertical mixing (Figure 6). However, the small changes in the climatology of OM4-cap relative to OM4 (despite large changes in the diurnal cycle of mixing) suggest that further improvements in the diurnal cycle might not have a large impact on climate of the OGCM.

Another potential candidate is the hybrid ($z_* - \sigma_2$) vertical coordinate in OM4. The σ_2 component of the coordinate leads to thicker layers (coarser vertical spacing in meters) in the western Pacific than in the eastern Pacific, since the top 200 m of the water column is much less stratified in density in the west (Figures 2 and 3). However, we conclude that this is not the primary source of remaining bias, since the OM4-up model shows a shallow thermocline bias in the western equatorial Pacific here with both with the hybrid (Figures 15 and 16) and z_* coordinate (i.e., Figure 10).

The MLE restratification parameterization also plays an important role in setting the mean the stratification in OM4. The tropical bias in OM4 was very sensitive to choices in MLE (not shown). However, this sensitivity is significantly reduced in OM4-up, suggesting there may have been some feedback between the original OM4 ePBL model and its MLE parameterization.

Another process we did not explore here is the impact of Langmuir turbulence, which is included in OM4 and ePBL (Reichl & Li, 2019) following the theory waves approach (Q. Li et al., 2017). The impact of Langmuir turbulence was not considered in the LES experiments of Whitt et al. (2022), so its parameterization and importance was not assessed in this work.

The role of horizontal resolution is another potentially important factor, especially due to its role in resolving TIWs and their mixing (Marchesiello et al., 2011). The source of the remaining shallow thermocline and EUC biases therefore remains unclear from this study, though forcing errors and additional mixing process biases are likely potential culprits. It is also likely that stratification biases that originate in other regions impact the equatorial solution, for example, driven by the representation of upwelling off the coast of South America (e.g., Jia et al., 2021), or by the representation of vertical mixing and solar penetration off-equator (W. Anderson et al., 2009).

We performed one further experiment in an effort to improve the simulation by enhancing the number of vertical grid levels by a factor of three. The OM4z_*-up-225 model is run with 225 vertical layers (increased from the original 75), where the OM4z_*-up-225 grid thicknesses start from the same 2 m spacing near the surface as OM4z_* (see Figure 1, red). The vertical grid spacing in OM4z_*-up-225 increases at depth much less rapidly than OM4, and it maintains relatively fine grid spacing throughout the upper 500 m. This yields a comparable increase in resolution to the study of Jia et al. (2021), which showed improvements in the representation of shear and stratification with 187 vertical levels compared to a control run with 51 vertical levels. Since the 225 level model is computationally more expensive (in terms of runtime and data storage), we only analyze it in the 10 years z_* experiments (1999–2008).

We first investigate the gradient Richardson number as resolved in the three experiments described previously (OM4z_*, OM4z_*-cap, and OM4z_*-up) at the four mooring sites (Figure 17), and investigate if increased low-Ri events are seen in OM4z_*-up-225. At each depth the Ri values are binned into 200 logarithmically spaced increments between $0.01 < Ri < 100$ for each of the four models, and in the following analysis we compare the counts of occurrences within each bin. Compared to the original OM4, OM4z_*-cap shows a slight increase in Ri < 0.25 (unstable) events within the top 30 m of the cold tongue (170°W–110°W). OM4z_*-up shows a further clear increase in Ri < 0.25 events extending all the way down to 200 m in the cold tongue, and a clear leftward (negative, destabilizing) shift of the Ri distribution at all depths relative to OM4z_*-cap. The vertical grid refinement in OM4z_*-up-225 has a minimal impact above the EUC core, but has a substantial impact throughout the lower flank of the EUC (below roughly 100 m), where we see a significant increase in low-Ri events at all four moorings. This result suggests that the Richardson number based vertical mixing parameterizations may require additional resolution, or additional parameterized mixing to compensate for coarse resolution, in order to improve simulation performance. This result is consistent with the findings of Jia et al. (2021), who found that increased vertical resolution yielded significantly more vertical shear across vertical wavenumber scales, leading to improved vertical mixing. It is likely that the reduced background viscosity plays a critical role in permitting these high wavenumber states, as we note a strong enhancement of shears in OM4z_*-up, and further enhancement with the refined resolution (note that Jia et al. (2021) used a background viscosity of 10^{-6} m^2 s^{-1}).

The impact of the additional vertical levels was fairly small for most other metrics, as summarized in Figure 10. Yet, one obvious improvement is an increase in the mean squared shear, and a realistic rightward expansion of the S^2 PDF toward higher shear values (increasing the mean and 80th percentile shear; compare the red and teal curves). Given that the time-mean currents are hardly impacted by the vertical refinement (top row of Figure 10), it is apparent that the increased S^2 in OM4z_*-up-225 must come from stronger transient shears. This does lead to some modulation of the deep stratification at certain depths, for example, capturing a local minimum in the thermostad and pycnostad around 200 m at 110°W. While the increase of interior transient shear and deep mixing events is an intriguing result, the additional levels do not significantly impact the depth of the thermocline in the west. This bias therefore remains an open question.

6. Conclusions and Outlooks

In this study we utilized a variety of methods to analyze causes of equatorial stratification and circulation biases (see Figures 2 and 3) in the NOAA Geophysical Fluid Dynamics Laboratory OM4 ocean model (Adcroft et al., 2019). We first compared the OM4 mixing parameterizations in a column model configuration of OM4 directly to LES (Whitt et al., 2022). This comparison led us to correct a significant bias in the diurnal cycle of mixing in OM4 (Section 3, Figure 6). However, when implementing the correction in the full three-dimensional ocean circulation model (OGCM), we found little impact on the time-mean biases. We did not investigate the impact of the improved diurnal cycle of mixing in a coupled ocean-atmosphere model (CGCM), where the atmospheric boundary layer has a chance to respond to the improvements in the oceanic boundary layer.

We found that the primary reason for OM4's stratification bias in the eastern equatorial Pacific was related to a high background viscosity, which results in poor simulation of the vertical shear that is used in the shear-based mixing parameterization. By eliminating the high background viscosity, we substantially improve the simulated stratification in this region (Figure 15). We also found that increasing the number of vertical layers in OM4 has the potential to significantly impact the mixing and improve interior stratification. Whether or not this stronger mixing results in improved currents compared to OM4 could not be evaluated using the present set of ocean

10.1029/2023EA003485

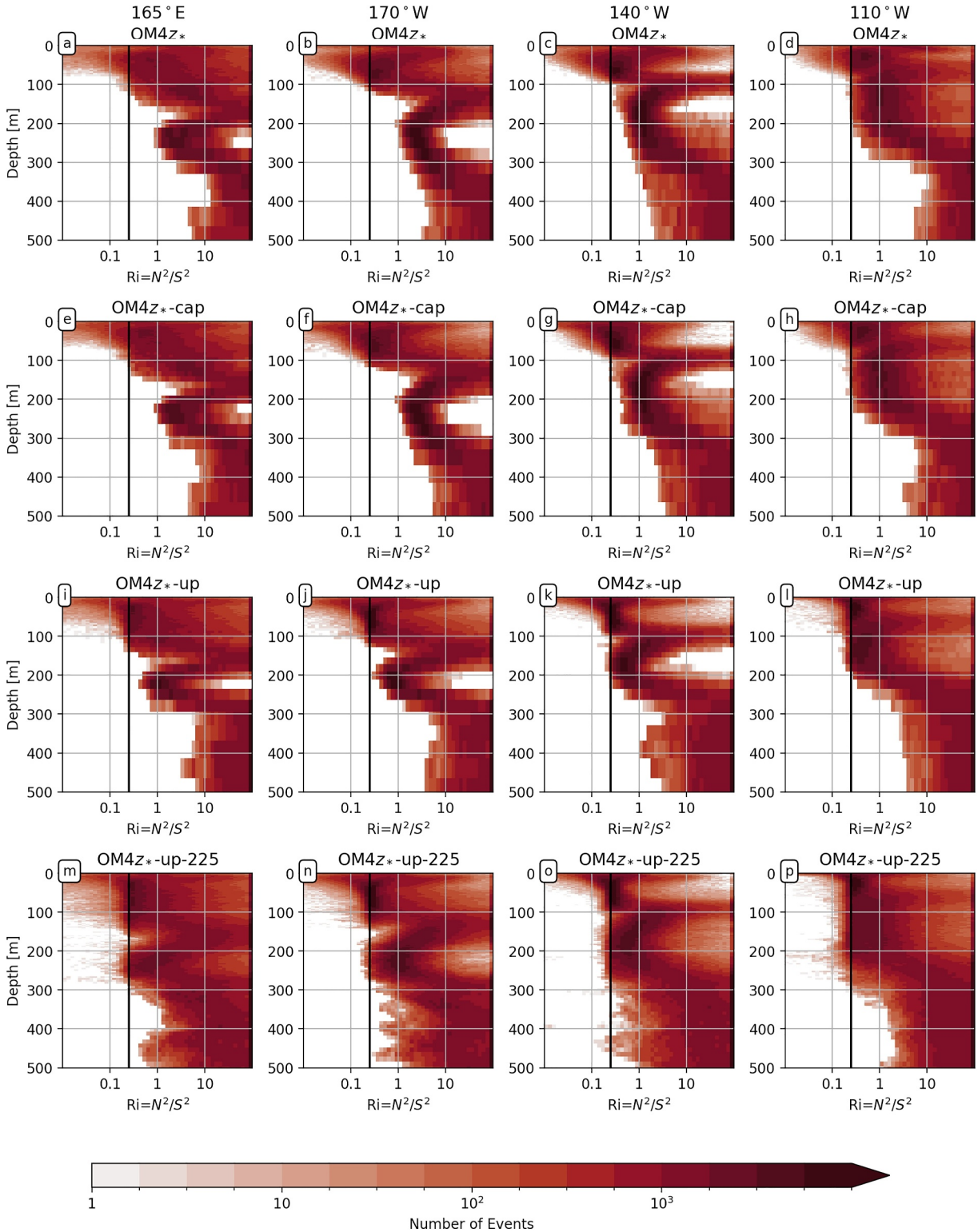

Figure 17. Number of discrete occurrence events, for each simulated Richardson number value (abscissa) and depth (ordinate), for the OM4z_* (a–d), OM4z_* with the ePBL m_* cap (e–h), OM4z_* with all updates presented in this manuscript (i–l), and the updated OM4z_* with higher vertical resolution (225 levels vs. 75 levels; (m–p)). The vertical black line is at Ri = 0.25.

observations, since the existing ADCP observations are limited to 50–250 m depths, while most of the simulation changes are seen between 250 and 500 m depths.

While our evaluation of these mixing parameterizations and their impacts on equatorial stratification has been specific to OM4, the potential implications of these results are much broader. First, we have demonstrated the importance of accurately simulating the EUC for capturing the mixing and equatorial stratification, and highlighted the importance of simulating the fully interactive and three-dimensional characteristics of this region. Second, we have emphasized the utility of the high-fidelity tropical LES (such as Whitt et al., 2022) for evaluating one-dimensional mixing parameterizations, despite the highly three-dimensional nature of this region (see also Large & Gent, 1999). We find that the one-dimensional model evaluations of ocean mixing parameterizations are an important complement to larger-scale OGCM experiments, and help guide parameterization sensitivity analysis.

Our analysis also revealed that vertical refinement of the ocean grid (using 225 rather than 75 layers) can lead to significantly richer transient shears and turbulence, and potentially reduced biases in mixing and variability. For future ocean model development, it will be important to consider whether an increased number of vertical layers is required and justified for simulating realistic turbulence and mixing, or if mixing parameterizations can be improved to enable more realistic simulations with coarser vertical grids. It is also likely that more optimal vertical coordinates (including hybrid approaches) can be devised that focus resolution in dynamically important regions. A challenge in vertical coordinate generation is that there is a delicate balance between the needs of resolving near-surface features (e.g., Pei et al., 2020) and baroclinic modes (e.g., Stewart et al., 2017), while preserving isopycnals and/or mitigating numerical mixing in regions of high stratification or overflows (Adcroft et al., 2019; Holmes et al., 2021). However, given the critical importance of the tropical oceans for global climate, variability, and change, and their strong impacts on the global atmosphere and surface fluxes which drive the global ocean circulation, further attention to the tropical ocean simulation is clearly warranted. In addition to considering the vertical grid spacing, there is also evidence that one needs to consider the model's horizontal resolution in order to simulate mean vertical shears that are consistent with observations (Jia et al., 2021).

Future work will investigate the impacts of these improved mixing schemes in CGCMs, to evaluate the hypothesis that the improvements in OM4 lead to improvements in tropical climate in a coupled climate model. Preliminary analysis of the OM4-up changes in developmental CGCMs at GFDL (not including CM4) indicate that the improved diurnal cycle and eastern Pacific stratification are also found in the CGCMs. These preliminary CGCM results have not yet shown any strong feedbacks from the atmospheric component that amplify or alter these ocean changes in coupled mode, but they do suggest that the atmospheric models, and model coupling, have their own biases that present further challenges for improving the equatorial ocean simulation in CGCMs. Outstanding issues include simulating the tropical patterns of winds, precipitation, clouds, and surface heat fluxes, all of which can strongly affect the response of the ocean component of a CGCM.

The present work demonstrates the utility of LES, the TAO network, and Argo floats for developing and evaluating OGCMs and CGCMs. Enhanced tropical observations to better constrain ocean mixing processes — for example, a redesigned Tropical Pacific Observing System (TPOS), and proposed TPOS Equatorial Pacific Experiment (TEPEX) field study, Kessler et al. (2021) — could greatly help to accelerate model development. The combination of long term and expansive data sets are a uniquely important tool for evaluating ocean climate model simulations, and should be combined with process based (e.g., LES) analysis methods to continue to evaluate and improve model biases.

Appendix A: Table of Acronyms and Symbols

See Table A1.

See Table A2.

Table A1
Commonly Used Acronyms and Symbols in the Paper

ADCP	Acoustic doppler current profiler
CGCM	coupled general circulation model
CM4	GFDL Climate Model 4
CMIP	Coupled Model Intercomparison Project 6
ENSO	El Niño/Southern Oscillation
ePBL	energetics-based planetary boundary layer
GFDL	Geophysical Fluid Dynamics Laboratory
JHL	Jackson et al. (2008) shear mixing
JRA55	Japanese 55-year Reanalysis
LES	large eddy simulation
MLE	mixed layer eddy parameterization
MOM6	Modular Ocean Model 6
OGCM	ocean general circulation model
OM4	Ocean and sea-ice Model 4
OMIP	Ocean Model Intercomparison Project
SIS2	Sea Ice Simulator 2
SST	sea surface temperature
TAO	Tropical Atmosphere Ocean moored buoy
TKE	turbulent kinetic energy
N^2	buoyancy frequency (Brunt-Väisälä)
S^2	shear frequency
Ri	Richardson number

Table A2
Model Experiment Naming Convention in the Paper

OM4	Global ocean model following Adcroft et al. (2019)
OM4-1d	single column model configuration of OM4
OM4z_*	z_* configuration of OM4
SMC/GLS	single column model configuration w/SMC/GLS mixing
OM4-cap	OM4 w/$m_* \leq 1.25$ cap
OM4-up	OM4 w/final updated model settings
OM4-225	OM4 w/increase to 225 vertical levels

Data Availability Statement

The source codes and model parameter settings needed for the SCM MOM6 experiments and the notebooks needed to generate the figures in this manuscript are available at Reichl (2024a). SCM and 3D processed output from MOM6 simulations are available at Reichl (2024b). LES and regional model data for the column model simulations were obtained by following the instructions of Whitt et al. (2022). Raw Argo data from the July 2023 data repository snapshot was used for this study (Argo, 2023). Gridded Argo data was obtained from http://sio-argo.ucsd.edu/RG_Climatology.html. TAO data was obtained from pmel.noaa.gov/gtmba/.

Acknowledgments
We thank Feiyu Lu and Matthew Harrison for helpful comments during internal reviews of this manuscript, as well as valuable comments from the anonymous reviewers. A. A. was supported by Award NA18OAR4320123 from the National Oceanic and Atmospheric Administration, U.S. Department of Commerce. We further acknowledge the support of Award GC22-207 from NOAA's Climate Program Office, Climate Variability and Predictability Program. The statements, findings, conclusions, and recommendations are those of the author(s) and do not necessarily reflect the views of the National Oceanic and Atmospheric Administration, or the U.S. Department of Commerce. We are extremely grateful to the programs that support the TAO mooring operation and its maintenance, including the GTMBA Project Office of NOAA/PMEL. We are also indebted to the many efforts of the Argo program, which provides data that were collected and made freely available by the International Argo Program and the national programs that contribute to it (http://www.argo.ucsd.edu, http://argo.jcommops.org). The Argo Program is part of the Global Ocean Observing System. We thank Dr. Daniel Whitt for conversations related to this work and for making the LES experiments presented in Whitt et al. (2022) easy to download and use. We acknowledge use of the colormaps from the cmocean package (Thyng et al., 2016).

References

Adcroft, A., Anderson, W., Balaji, V., Blanton, C., Bushuk, M., Dufour, O., et al. (2019). The GFDL Global Ocean and Sea ice model OM4.0: Model description and simulation features. *Journal of Advances in Modeling Earth Systems*, *11*(10), 3167–3211. https://doi.org/10.1029/2019MS001726

Anderson, S. P., Weller, R. A., & Lukas, R. B. (1996). Surface buoyancy forcing and the mixed layer of the Western Pacific warm pool: Observations and 1D model results. *Journal of Climate*, *9*(12), 3056–3085. https://doi.org/10.1175/1520-0442(1996)009⟨3056:SBFATM⟩2.0.CO;2

Anderson, W., Gnanadesikan, A., & Wittenberg, A. (2009). Regional impacts of ocean color on tropical Pacific variability. *Ocean Science*, *5*, 313–327. https://doi.org/10.5194/osd-6-243-2009

Argo. (2023). *Argo float data and metadata from Global Data Assembly Centre (Argo GDAC)*. SEANOE. https://doi.org/10.17882/42182

Chang, Y.-S., Zhang, S., Rosati, A., Delworth, T. L., & Stern, W. F. (2013). An assessment of oceanic variability for 1960–2010 from the GFDL ensemble coupled data assimilation. *Climate Dynamics*, *40*(3–4), 775–803. https://doi.org/10.1007/s00382-012-1412-2

Cherian, D. A., Whitt, D. B., Holmes, R. M., Lien, R.-C., Bachman, S. D., & Large, W. G. (2021). Off-equatorial deep-cycle turbulence forced by tropical instability waves in the equatorial Pacific. *Journal of Physical Oceanography*, *51*(5), 1575–1593. https://doi.org/10.1175/JPO-D-20-0229.1

Chiodi, A. M., & Harrison, D. E. (2017). Simulating ENSO SSTAs from TAO/TRITON winds: The impacts of 20 Years of buoy observations in the Pacific waveguide and comparison with reanalysis products. *Journal of Climate*, *30*(3), 1041–1059. https://doi.org/10.1175/JCLI-D-15-0865.1

D'Asaro, E. A. (2014). Turbulence in the upper-ocean mixed layer. *Annual Review of Marine Science*, *6*(1), 101–115. https://doi.org/10.1146/annurev-marine-010213-135138

Delworth, T. L., Cooke, W. F., Adcroft, A., Bushuk, M., Chen, J., Dunne, K. A., et al. (2020). Spear: The next generation GFDL modeling system for seasonal to multidecadal prediction and projection. *Journal of Advances in Modeling Earth Systems*, *12*(3), e2019MS001895. https://doi.org/10.1029/2019MS001895

Dunne, J. P., Horowitz, L. W., Adcroft, A. J., Ginoux, P., Held, I. M., John, J. G., et al. (2020). The GFDL Earth System Model version 4.1 (GFDL-ESM 4.1): Overall coupled model description and simulation characteristics. *Journal of Advances in Modeling Earth Systems*, *12*(11), e2019MS002015. https://doi.org/10.1029/2019MS002015

Eyring, V., Bony, S., Meehl, G. A., Senior, C. A., Stevens, B., Stouffer, R. J., & Taylor, K. E. (2016). Overview of the Coupled Model Intercomparison Project phase 6 (CMIP6) experimental design and organization. *Geoscientific Model Development*, *9*(5), 1937–1958. https://doi.org/10.5194/gmd-9-1937-2016

Farneti, R., Stiz, A., & Ssebandeke, J. B. (2022). Improvements and persistent biases in the Southeast tropical Atlantic in CMIP models. *npj Climate and Atmospheric Science*, *5*(1), 42. https://doi.org/10.1038/s41612-022-00264-4

Fox-Kemper, B., Adcroft, A., Böning, C. W., Chassignet, E. P., Curchitser, E., Danabasoglu, G., et al. (2019). Challenges and prospects in ocean circulation models. *Frontiers in Marine Science*, *6*, 65. https://doi.org/10.3389/fmars.2019.00065

Fox-Kemper, B., Danabasoglu, G., Ferrari, R., Griffies, S., Hallberg, R., Holland, M., et al. (2011). Parameterization of mixed layer eddies. III: Implementation and impact in global ocean climate simulations. *Ocean Modelling*, *39*(1–2), 61–78. https://doi.org/10.1016/j.ocemod.2010.09.002

Fox-Kemper, B., Johnson, L., & Qiao, F. (2022). Ocean near-surface layers. In *Ocean mixing* (pp. 65–94). Elsevier. https://doi.org/10.1016/B978-0-12-821512-8.00011-6

Gnanadesikan, A., & Anderson, W. G. (2009). Ocean water clarity and the Ocean general circulation in a coupled climate model. *Journal of Physical Oceanography*, *39*(2), 314–332. https://doi.org/10.1175/2008JPO3935.1

Gregg, M. C., Peters, H., Wesson, J. C., Oakey, N. S., & Shay, T. J. (1985). Intensive measurements of turbulence and shear in the equatorial undercurrent. *Nature*, *318*(6042), 140–144. https://doi.org/10.1038/318140a0

Griffies, S. M., Danabasoglu, G., Durack, P. J., Adcroft, A. J., Balaji, V., Böning, C. W., et al. (2016). OMIP contribution to CMIP6: Experimental and diagnostic protocol for the physical component of the Ocean Model Intercomparison Project. *Geoscientific Model Development*, *9*(9), 3231–3296. https://doi.org/10.5194/gmd-9-3231-2016

Griffies, S. M., & Hallberg, R. W. (2000). Biharmonic friction with a Smagorinsky-like viscosity for use in large-scale eddy-permitting ocean models. *Monthly Weather Review*, *128*(8), 2935–2946. https://doi.org/10.1175/1520-0493(2000)128⟨2935:BFWASL⟩2.0.CO;2

Guilyardi, E., Capotondi, A., Lengaigne, M., Thual, S., & Wittenberg, A. T. (2020). ENSO modeling: History, progress, and challenges. In M. J. McPhaden, A. Santoso, & W. Cai (Eds.), *Geophysical monograph series* (1st ed., pp. 199–226). Wiley. https://doi.org/10.1002/9781119548164.ch9

Harrison, M. J., & Hallberg, R. W. (2008). Pacific subtropical cell response to reduced equatorial dissipation. *Journal of Physical Oceanography*, *38*(9), 1894–1912. https://doi.org/10.1175/2008JPO3708.1

Hawkins, E., & Sutton, R. (2009). The potential to narrow uncertainty in regional climate predictions. *Bulletin of the American Meteorological Society*, *90*(8), 1095–1108. https://doi.org/10.1175/2009BAMS2607.1

Held, I. M., Guo, H., Adcroft, A., Dunne, J. P., Horowitz, L. W., Krasting, J., et al. (2019). Structure and performance of GFDL's CM4.0 climate model. *Journal of Advances in Modeling Earth Systems*, *11*(11), 3691–3727. https://doi.org/10.1029/2019MS001829

Hewitt, H. T., Roberts, M., Mathiot, P., Biastoch, A., Blockley, E., Chassignet, E. P., et al. (2020). Resolving and parameterising the ocean mesoscale in Earth system models. *Current Climate Change Reports*, *6*(4), 137–152. https://doi.org/10.1007/s40641-020-00164-w

Holmes, R. M., & Thomas, L. N. (2015). The modulation of equatorial turbulence by tropical instability waves in a regional Ocean Model. *Journal of Physical Oceanography*, *45*(4), 1155–1173. https://doi.org/10.1175/JPO-D-14-0209.1

Holmes, R. M., Zika, J. D., Griffies, S. M., Hogg, A. M., Kiss, A. E., & England, M. H. (2021). The geography of numerical mixing in a suite of Global Ocean models. *Journal of Advances in Modeling Earth Systems*, *13*(7), e2020MS002333. https://doi.org/10.1029/2020MS002333

Hughes, K. G., Moum, J. N., & Shroyer, E. L. (2020). Evolution of the velocity structure in the diurnal warm layer. *Journal of Physical Oceanography*, *50*(3), 615–631. https://doi.org/10.1175/JPO-D-19-0207.1

IPCC. (2021). Climate change 2021: The physical science basis. In *Contribution of working Group I to the sixth assessment report of the intergovernmental panel on climate change (Vol. In Press) [Book]*. Cambridge University Press. https://doi.org/10.1017/9781009157896

Jackson, L., Hallberg, R., & Legg, S. (2008). A parameterization of shear-driven turbulence for ocean climate models. *Journal of Physical Oceanography*, *38*(5), 1033–1053. https://doi.org/10.1175/2007JPO3779.1

Jia, Y., Richards, K. J., & Annamalai, H. (2021). The impact of vertical resolution in reducing biases in sea surface temperature in a tropical Pacific Ocean model. *Ocean Modelling*, *157*, 101722. https://doi.org/10.1016/j.ocemod.2020.101722

Jochum, M., & Murtugudde, R. (2006). Temperature advection by tropical instability waves. *Journal of Physical Oceanography*, *36*(4), 592–605. https://doi.org/10.1175/JPO2870.1

Kessler, W. S. (2006). The circulation of the Eastern tropical Pacific: A review. *Progress in Oceanography*, *69*(2–4), 181–217. https://doi.org/10.1016/j.pocean.2006.03.009

Kessler, W. S., Cravatte, S., Strutton, P. G., Sutton, A. J., Kumar, A., Takaya, Y., et al. (2021). Final report of TPOS 2020 (Tech. Rep. No. 268). *UNESCO IOC Global Ocean Observing System (GOOS)*. https://tropicalpacific.org/tpos2020-project-archive/reports

Large, W. G., & Gent, P. R. (1999). Validation of vertical mixing in an equatorial Ocean Model using large eddy simulations and observations. *Journal of Physical Oceanography*, *29*(3), 449–464. https://doi.org/10.1175/1520-0485(1999)029⟨0449:VOVMIA⟩2.0.CO;2

Large, W. G., McWilliams, J. C., & Doney, S. C. (1994). Oceanic vertical mixing: A review and a model with a nonlocal boundary layer parameterization. *Reviews of Geophysics*, *32*(4), 363–403. https://doi.org/10.1029/94RG01872

Large, W. G., & Yeager, S. G. (2009). The global climatology of an Interannually varying air–sea flux data set. *Climate Dynamics*, *33*(2–3), 341–364. https://doi.org/10.1007/s00382-008-0441-3

L'Heureux, M. L., Tippett, M. K., & Barnston, A. G. (2015). Characterizing ENSO coupled variability and its impact on North American seasonal precipitation and temperature. *Journal of Climate*, *28*(10), 4231–4245. https://doi.org/10.1175/JCLI-D-14-00508.1

Li, G., & Xie, S.-P. (2012). Origins of tropical-wide SST biases in CMIP multi-model ensembles: TROPICAL-WIDE SST biases in models. *Geophysical Research Letters*, *39*(22), L22703. https://doi.org/10.1029/2012GL053777

Li, G., & Xie, S.-P. (2014). Tropical biases in CMIP5 multimodel ensemble: The excessive equatorial Pacific cold tongue and double ITCZ problems. *Journal of Climate*, *27*(4), 1765–1780. https://doi.org/10.1175/JCLI-D-13-00337.1

Li, Q., Fox-Kemper, B., Breivik, Ø., & Webb, A. (2017). Statistical models of global Langmuir mixing. *Ocean Modelling*, *113*, 95–114. https://doi.org/10.1016/j.ocemod.2017.03.016

Li, Q., Reichl, B. G., Fox-Kemper, B., Adcroft, A. J., Belcher, S. E., Danabasoglu, G., et al. (2019). Comparing Ocean surface boundary vertical mixing schemes including Langmuir turbulence. *Journal of Advances in Modeling Earth Systems*, *11*(11), 3545–3592. https://doi.org/10.1029/2019MS001810

Li, X., Cai, W., Meehl, G. A., Chen, D., Yuan, X., Raphael, M., et al. (2021). Tropical teleconnection impacts on Antarctic climate changes. *Nature Reviews Earth & Environment*, *2*(10), 680–698. https://doi.org/10.1038/s43017-021-00204-5

Locarnini, R. A., Mishonov, A. V., Antonov, J. I., Boyer, T. P., & Garcia, H. E. (2006). *World Ocean Atlas 2005, volume 1: Temperature (Tech. Rep. No. NOAA Atlas NESDIS 61)*. U.S. Government Printing Office.

Manizza, M., Le Quéré, C., Watson, A. J., & Buitenhuis, E. T. (2005). Bio-optical feedbacks among phytoplankton, upper ocean physics and sea-ice in a global model. *Geophysical Research Letters*, *32*(5), L05603. https://doi.org/10.1029/2004GL020778

Marchesiello, P., Capet, X., Menkes, C., & Kennan, S. C. (2011). Submesoscale dynamics in tropical instability waves. *Ocean Modelling*, *39*(1–2), 31–46. https://doi.org/10.1016/j.ocemod.2011.04.011

Masich, J., Kessler, W. S., Cronin, M. F., & Grissom, K. R. (2021). Diurnal cycles of near-surface currents across the tropical Pacific. *Journal of Geophysical Research: Oceans*, *126*(4), e2020JC016982. https://doi.org/10.1029/2020JC016982

McPhaden, M. J., Santoso, A., & Cai, W. (2020). *El Niño southern oscillation in a changing climate* (Vol. 253). Wiley. https://doi.org/10.1002/9781119548164

Meehl, G. A., Gent, P. R., Arblaster, J. M., Otto-Bliesner, B. L., Brady, E. C., & Craig, A. (2001). Factors that affect the amplitude of El Nino in global coupled climate models. *Climate Dynamics*, *17*(7), 515–526. https://doi.org/10.1007/PL00007929

Miles, J. W. (1961). On the stability of Heterogeneous shear flows. *Journal of Fluid Mechanics*, *10*(04), 496. https://doi.org/10.1017/S0022112061000305

Mishonov, A. V., Locarnini, R. A., Boyer, T. P., Mishonov, A. V., & Garcia, H. E. (2006). *World Ocean Atlas 2005, volume 2: Salinity (Tech. Rep. No. NOAA Atlas NESDIS 62)*. U.S. Government Printing Office.

Moum, J. N., & Caldwell, D. R. (1985). Local influences on shear-flow turbulence in the equatorial ocean. *Science*, *230*(4723), 315–316. https://doi.org/10.1126/science.230.4723.315

Moum, J. N., Hughes, K. G., Shroyer, E. L., Smyth, W. D., Cherian, D., Warner, S. J., et al. (2022). Deep cycle turbulence in Atlantic and Pacific cold tongues. *Geophysical Research Letters*, *49*(8), e2021GL097345. https://doi.org/10.1029/2021GL097345

Moum, J. N., Nash, J. D., & Smyth, W. D. (2011). Narrowband oscillations in the upper equatorial ocean. Part I: Interpretation as shear instabilities. *Journal of Physical Oceanography*, *41*(3), 397–411. https://doi.org/10.1175/2010JPO4450.1

Moum, J. N., Perlin, A., Nash, J. D., & McPhaden, M. J. (2013). Seasonal sea surface cooling in the equatorial Pacific cold tongue controlled by ocean mixing. *Nature*, *500*(7460), 64–67. https://doi.org/10.1038/nature12363

Palmer, T., Shutts, G., Hagedorn, R., Doblas-Reyes, F., Jung, T., & Leutbecher, M. (2005). Representing model uncertainty in weather and climate prediction. *Annual Review of Earth and Planetary Sciences*, *33*(1), 163–193. https://doi.org/10.1146/annurev.earth.33.092203.122552

Pei, S., Shinoda, T., Wang, W., & Lien, R. (2020). Simulation of deep cycle turbulence by a Global Ocean general circulation model. *Geophysical Research Letters*, *47*(15), e2020GL088384. https://doi.org/10.1029/2020GL088384

Peters, H., Gregg, M. C., & Sanford, T. B. (1994). The diurnal cycle of the upper equatorial ocean: Turbulence, fine-scale shear, and mean shear. *Journal of Geophysical Research*, *99*(C4), 7707–7723. https://doi.org/10.1029/93JC03506

Pham, H. T., Sarkar, S., & Winters, K. B. (2013). Large-eddy simulation of deep-cycle turbulence in an equatorial undercurrent model. *Journal of Physical Oceanography*, *43*(11), 2490–2502. https://doi.org/10.1175/JPO-D-13-016.1

Price, J. F., Weller, R. A., & Pinkel, R. (1986). Diurnal cycling: Observations and models of the upper ocean response to diurnal heating, cooling, and wind mixing. *Journal of Geophysical Research*, *91*(C7), 8411–8427. https://doi.org/10.1029/JC091iC07p08411

Pujiana, K., Moum, J. N., & Smyth, W. D. (2018). The role of turbulence in redistributing upper-ocean heat, freshwater, and momentum in response to the MJO in the equatorial Indian ocean. *Journal of Physical Oceanography*, *48*(1), 197–220. https://doi.org/10.1175/JPO-D-17-0146.1

Reichl, B. G. (2024a). Breichl/EqPac_Paper: V1.0.0 (v1.0.0) [Software]. *Zenodo*. https://doi.org/10.5281/zenodo.12764418

Reichl, B. G. (2024b). MOM6 model output from "improving Upper Ocean Vertical mixing in the equatorial oceans in the NOAA/GFDL OM4 model [Dataset]. *Zenodo*. https://doi.org/10.5281/zenodo.10406423

Reichl, B. G., & Hallberg, R. (2018). A simplified energetics based Planetary Boundary Layer (ePBL) approach for ocean climate simulations. *Ocean Modelling*, *132*, 112–129. https://doi.org/10.1016/j.ocemod.2018.10.004

Reichl, B. G., & Li, Q. (2019). A parameterization with a constrained potential energy conversion rate of vertical mixing due to Langmuir turbulence. *Journal of Physical Oceanography*, *49*(11), 2935–2959. https://doi.org/10.1175/JPO-D-18-0258.1

Richards, K. J., Xie, S.-P., & Miyama, T. (2009). Vertical mixing in the ocean and its impact on the coupled ocean–atmosphere system in the Eastern tropical Pacific. *Journal of Climate*, *22*(13), 3703–3719. https://doi.org/10.1175/2009JCLI2702.1

Roemmich, D., & Gilson, J. (2009). The 2004–2008 mean and annual cycle of temperature, salinity, and steric height in the global ocean from the Argo Program. *Progress in Oceanography*, *82*(2), 81–100. https://doi.org/10.1016/j.pocean.2009.03.004

Rohr, J. J., Itsweire, E. C., Helland, K. N., & Atta, C. W. V. (1988). Growth and decay of turbulence in a stably stratified shear flow. *Journal of Fluid Mechanics*, *195*(1), 77. https://doi.org/10.1017/S0022112088002332

Ropelewski, C. F., & Halpert, M. S. (1987). Global and regional scale precipitation patterns associated with the El Niño/Southern oscillation. *Monthly Weather Review*, *115*(8), 1606–1626. https://doi.org/10.1175/1520-0493(1987)115⟨1606:GARSPP⟩2.0.CO;2

Seo, H., Jochum, M., Murtugudde, R., Miller, A. J., & Roads, J. O. (2007). Feedback of tropical instability-wave-induced atmospheric variability onto the ocean. *Journal of Climate*, *20*(23), 5842–5855. https://doi.org/10.1175/JCLI4330.1

Small, R., de Szoeke, S., Xie, S., O'Neill, L., Seo, H., Song, Q., et al. (2008). Air–sea interaction over ocean fronts and eddies. *Dynamics of Atmospheres and Oceans*, *45*(3–4), 274–319. https://doi.org/10.1016/j.dynatmoce.2008.01.001

Smyth, W. D., & Moum, J. N. (2013). Marginal instability and deep cycle turbulence in the Eastern equatorial Pacific Ocean. *Geophysical Research Letters*, *40*(23), 6181–6185. https://doi.org/10.1002/2013GL058403

Smyth, W. D., Moum, J. N., Li, L., & Thorpe, S. A. (2013). Diurnal shear instability, the descent of the surface shear layer, and the deep cycle of equatorial turbulence. *Journal of Physical Oceanography*, *43*(11), 2432–2455. https://doi.org/10.1175/JPO-D-13-089.1

Smyth, W. D., Moum, J. N., & Nash, J. D. (2011). Narrowband oscillations in the upper equatorial ocean. Part II: Properties of shear instabilities. *Journal of Physical Oceanography*, *41*(3), 412–428. https://doi.org/10.1175/2010JPO4451.1

Sprintall, J., Cravatte, S., Dewitte, B., Du, Y., & Gupta, A. S. (2020). ENSO oceanic teleconnections. In M. J. McPhaden, A. Santoso, & W. Cai (Eds.), *Geophysical monograph series* (1st ed., pp. 337–359). Wiley. https://doi.org/10.1002/9781119548164.ch15

Stewart, K., Hogg, A., Griffies, S., Heerdegen, A., Ward, M., Spence, P., & England, M. (2017). Vertical resolution of Baroclinic modes in global ocean models. *Ocean Modelling*, *113*, 50–65. https://doi.org/10.1016/j.ocemod.2017.03.012

Sun, C., Smyth, W. D., & Moum, J. N. (1998). Dynamic instability of stratified shear flow in the upper equatorial Pacific. *Journal of Geophysical Research*, *103*(C5), 10323–10337. https://doi.org/10.1029/98JC00191

Sun, Z., Liu, H., Lin, P., Tseng, Y., Small, J., & Bryan, F. (2019). The modeling of the north equatorial countercurrent in the community Earth system model and its oceanic component. *Journal of Advances in Modeling Earth Systems*, *11*(2), 531–544. https://doi.org/10.1029/2018MS001521

Taboada, F. G., Stock, C. A., Griffies, S. M., Dunne, J., John, J. G., Small, R. J., & Tsujino, H. (2019). Surface winds from atmospheric reanalysis lead to contrasting oceanic forcing and coastal upwelling patterns. *Ocean Modelling*, *133*, 79–111. https://doi.org/10.1016/j.ocemod.2018.11.003

Taschetto, A. S., Ummenhofer, C. C., Stuecker, M. F., Dommenget, D., Ashok, K., Rodrigues, R. R., & Yeh, S. (2020). ENSO atmospheric teleconnections. In M. J. McPhaden, A. Santoso, & W. Cai (Eds.), *Geophysical monograph series* (1st ed., pp. 309–335). Wiley. https://doi.org/10.1002/9781119548164.ch14

Thyng, K., Greene, C., Hetland, R., Zimmerle, H., & DiMarco, S. (2016). True colors of oceanography: Guidelines for effective and accurate colormap selection. *Oceanography*, *29*(3), 9–13. https://doi.org/10.5670/oceanog.2016.66

Tozuka, T., Ohishi, S., & Cronin, M. F. (2018). A metric for surface heat flux effect on horizontal sea surface temperature gradients. *Climate Dynamics*, *51*(1–2), 547–561. https://doi.org/10.1007/s00382-017-3940-2

Trenberth, K. E., Branstator, G. W., Karoly, D., Kumar, A., Lau, N.-C., & Ropelewski, C. (1998). Progress during TOGA in understanding and modeling global teleconnections associated with tropical sea surface temperatures. *Journal of Geophysical Research*, *103*(C7), 14291–14324. https://doi.org/10.1029/97JC01444

Tsujino, H., Urakawa, L. S., Griffies, S. M., Danabasoglu, G., Adcroft, A. J., Amaral, A. E., et al. (2020). Evaluation of global ocean–sea-ice model simulations based on the experimental protocols of the Ocean Model Intercomparison Project phase 2 (OMIP-2). *Geoscientific Model Development*, *13*(8), 3643–3708. https://doi.org/10.5194/gmd-13-3643-2020

Tsujino, H., Urakawa, S., Nakano, H., Small, R. J., Kim, W. M., Yeager, S. G., et al. (2018). JRA-55 based surface dataset for driving ocean–sea-ice models (JRA55-do). *Ocean Modelling*, *130*, 79–139. https://doi.org/10.1016/j.ocemod.2018.07.002

Umlauf, L., & Burchard, H. (2003). A generic length-scale equation for geophysical turbulence models. *Journal of Marine Research*, *61*(2), 235–265. https://doi.org/10.1357/002224003322005087

Voldoire, A., Exarchou, E., Sanchez-Gomez, E., Demissie, T., Deppenmeier, A.-L., Frauen, C., et al. (2019). Role of wind stress in driving SST biases in the Tropical Atlantic. *Climate Dynamics*, *53*(5–6), 3481–3504. https://doi.org/10.1007/s00382-019-04717-0

Wang, D., Large, W. G., & McWilliams, J. C. (1996). Large-eddy simulation of the equatorial ocean boundary layer: Diurnal cycling, eddy viscosity, and horizontal rotation. *Journal of Geophysical Research*, *101*(C2), 3649–3662. https://doi.org/10.1029/95JC03441

Wang, D., McWilliams, J. C., & Large, W. G. (1998). Large-eddy simulation of the diurnal cycle of deep equatorial turbulence. *Journal of Physical Oceanography*, *28*(1), 129–148. https://doi.org/10.1175/1520-0485(1998)028⟨0129:LESOTD⟩2.0.CO;2

Warner, S. J., & Moum, J. N. (2019). Feedback of mixing to ENSO phase change. *Geophysical Research Letters*, *46*(23), 13920–13927. https://doi.org/10.1029/2019GL085415

Wenegrat, J. O., & McPhaden, M. J. (2015). Dynamics of the surface layer diurnal cycle in the equatorial Atlantic Ocean (0°, 23°W). *Journal of Geophysical Research: Oceans*, *120*(1), 563–581. https://doi.org/10.1002/2014JC010504

Whitt, D. B., Cherian, D. A., Holmes, R. M., Bachman, S. D., Lien, R.-C., Large, W. G., & Moum, J. N. (2022). Simulation and scaling of the turbulent vertical heat transport and deep-cycle turbulence across the equatorial Pacific cold tongue. *Journal of Physical Oceanography*, *52*(5), 981–1014. https://doi.org/10.1175/JPO-D-21-0153.1